Fall 2008

A Systematic Study on Structural and Optical Properties in Conjugated Polymer Photovoltaic Devices

Sri Sabarinadh Sunkavalli
Old Dominion University

A SYSTEMATIC STUDY ON STRUCTURAL AND OPTICAL PROPERTIES IN CONJUGATED POLYMER PHOTOVOLTAIC DEVICES

by

Sri Sabarinadh Sunkavalli

B.E. June 2002, CRR College of Engineering

A Thesis Submitted to the Faculty of

Old Dominion University in Partial Fulfillment of the

Requirement for the Degree of

MASTER OF SCIENCE

ELECTRICAL ENGINEERING

OLD DOMINION UNIVERSITY

DECEMBER 2008

Approved by:

Gon Namkoong (Director)

Abdel Tarek Fattah (Member)

Helmut Baumgart (Member)

ABSTRACT

A SYSTEMATIC STUDY ON STRUCTURAL AND OPTICAL PROPERTIES IN CONJUGATED POLYMER PHOTOVOLTAIC DEVICES

Sri Sabarinadh Sunkavalli
Old Dominion University, 2008
Director: Dr. Gon Namkoong

Conjugated polymer/fullerene based solar cells represent an exciting alternative to inorganic ones because of their low production costs, flexibility and low weight. At present, commercialization of organic photovoltaic (OPV) cells is limited due to their relatively low efficiency in comparison to silicon ones. In order to understand the operation of OPV cells and to increase their efficiency, more information about the structure of the absorber layer is needed. In particular, the connection between structure and properties of the absorber layer is of great importance. Performance of bulk heterojunction organic solar cells based on poly (3-hexylthiophene) as donor and a soluble fullerene PCBM (C_{60} or C_{70}) as acceptor is strongly influenced by active layer morphology. Optimized high temperature annealing under nitrogen atmosphere leads to a well-defined nanoscale (< 5 nm) interpenetrating network. Films made of organic blend by mixing P3HT, PCBM are annealed at different temperatures. Improvement in film morphology upon annealing results in enhanced photovoltaic device performance. This enhanced device performance is thought to be due partly to the improvement in the interfacial contact between the metal electrode and the active layer. Upon annealing the roughness of the active layer increases and becomes highest at 150^0C. To elucidate the

nanomorphology, atomic force microscopy (AFM) is used. Morphology studies and roughness analysis of the blend films (P3HT:PCBM-C_{70}) indicated that excellent miscibility between polymer and PCBM favors exciton separation and improved absorption spectrum. The aim of this work was to study the correlation between structural, optical and transport properties of conjugated polymer/fullerene films. We start by investigating of pristine polythiophene films. From spectroscopic ellipsometry studies it follows, that the polythiophene films consist of a highly ordered interface layer. A correlation between the surface roughness and absorption was shown. After this, the polythiophene/fullerene films were investigated. We found that annealing of such films supports the formation of polythiophene crystallites due to enhanced diffusion of fullerene at elevated temperatures. The crystallization of polythiophene leads to an increased optical absorption in the visible region due to stronger interchain interaction between polythiophene molecules. The observed increase of the efficiency of the polythiophene/ fullerene solar cells after annealing was explained by improved optical absorption together with improved hole mobility.

This thesis is dedicated to my family.

ACKNOWLEDGEMENTS

There are several people who significantly influenced this thesis in many ways and I would like to thank them here. First and foremost my advisor, Dr. Gon Namkoong provides me complete freedom to focus on my research problems that interest, and for that I am very grateful. His enthusiasm and genuine interest in my progress made my job easy and stress free. His nanostructures course had a direct impact on my research. I am thankful that he taught me organizational skills and work ethics.

I am particularly indebted to Dr. Abdel Tarek Fattah for providing valuable suggestions, feedback and patiently explaining organic chemistry to me. For many interesting and exciting discussions of inorganic and organic photovoltaic's I want to thank Dr. Helmut Baumgart. I am lucky to work with an incredible group of students at Applied Research Center, and it has been a joy to socialize, talk and learn from Mr Sampath Chennuri, Mr Kurniawan Foe, Mr Pat Boland and Joe Wie. I have benefited greatly from numerous discussions and arguments. My special thanks to Dr. Diefeng Gu and Dr. Wie Cao for the fruitful discussions, the advice and their contribution to the measurements.

I would like to thank my best friends Hanu, Mahi, Murthy, Pansi, Raji, Suri, Srinu, Uppi, Uma and Venu. I am deeply and forever indebted to my parents for their love support and encouragement throughout my entire life. I am also very grateful to my sister Sujatha, my little brother Viswanadh and Vinod for being a constant source of support and for continuously reminding me to graduate.

TABLE OF CONTENTS

LIST OF TABLES

LIST OF FIGURES

Figure Page

Figure Page

Figure Page

Figure Page

CHAPTER I

INTRODUCTION

Solar energy has been touted for years as a safer, cleaner alternative to fossil fuels to meet rising energy demands. Producing electricity from solar cells reduces air pollutants by about 90% [1] in comparison to using conventional fossil fuel technologies.

Solar cells known as photovoltaic cells convert one form of energy (sunlight) into another form of energy (electricity). Most solar cells are made from silicon. Silicon has dual properties of metal as well as insulator. Atoms in a metal have loosely bound electrons that flow easily when a voltage, or electrical pressure, is applied. Atoms in an insulator have tightly bound electrons that cannot flow even when a strong electric voltage is applied. Atoms in a semiconductor bind their electrons somewhat more tightly than metals but more loosely than insulators. Their electrical conductivity can be varied by a factor of thousands by introducing small amounts of impurities, or "**dopants**" into the semiconductor structure.

Conversion of sunlight to electricity starts at the atomic level when light composed of energy particles called photons flows from the sun and strikes the solar cell. As each photon strikes a silicon atom, it ionizes the atom by transferring its energy to an outer electron, allowing it to break free from outer orbitals. The energy of the photon is converted into electron movement energy called electric current. Another reason to use silicon in solar cells is because the energy needed to ionize a silicon electron matches the typical energy of photons coming from our sun.

Solar cells perform the conversion without moving parts, noise, pollution, radiation or maintenance, but there are some issues regarding the environment and health. Manufacturing of solar cells needs dangerous materials like arsenic and silicon, which is dangerous when inhaled for long time. Limited availability of silicon brought organic semiconducting materials into the picture. Figure 1 shows how silicon demand was high and how supply lasted before 2008.

This Journal model used for this document is IEEE Transactions on Neural Networks.

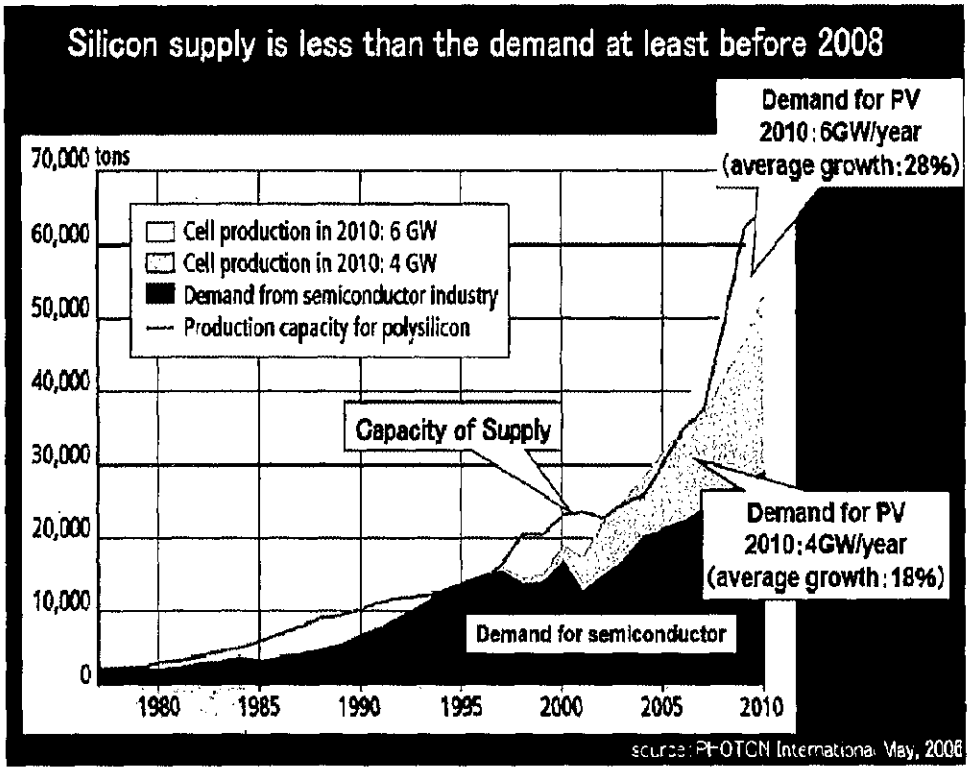

Figure 1.1. Supply - Demand curve for silicon. Silicon supply demand is less before 2008 [4].

Organic semiconductors have gained a lot of attention during the past few years, driven by the potential for applications as low cost electronic materials like sensors [10], photodetectors [11], light emitting diodes [8], memory devices [9] and solar cells [5]. Organic materials bear the potential to develop a long-term technology that is economically viable for large-scale power generation based on environmentally safe materials with unlimited availability. Organic semiconductors and carbon nanomaterials, especially fullerene derivatives, have attracted much interest because of their novel structures, properties and potential applications. Organic photovoltaics are promising alternatives to their inorganic counterparts [7]. The table below shows the main differences between inorganic and organic semiconducting materials used in the present photovoltaics market.

Table 1.1. Main differences between organic/ inorganic semiconductor materials used in PV [2].

	Crystalline Silicon	**Organic**
Basic Entries	Atoms	Molecules
Bulk structure	Crystalline	Amorphous
Dielectric constants	11.9	~ 3-4
Excitation binding energies at room temperature (k_BT)	26meV	2eV
Dominant transport mechanism	Band transport	Hopping
Charge carrier mobility μ	100-1000 cm^2/Vs	<0.1 cm^2/Vs
Absorption coefficient	2500/cm	16000/cm
T – dependence of mobility	T↑ ➔ μ↓	T↑ ➔ μ↑

The field of organic photovoltaics (OPVs) is comprised organic/inorganic nanostructures like dye sensitized solar cells, multilayers of small organic molecules, and phase-separated mixtures of organic materials (the bulk heterojunction solar cell). Light absorption in organic solar cells leads to the generation of excited, bound electron– hole pairs often called excitons. To achieve substantial energy conversion efficiencies, these excited electron–hole pairs need to be dissociated into free charge carriers with a high yield. Excitons can be dissociated at interfaces of materials with different electron affinities or by electric fields, or the dissociation can be trap or impurity assisted. Blending conjugated polymers with high-electron-affinity molecules like C_{60} has proven to be an efficient way for rapid exciton dissociation. Conjugated polymer C_{60} interpenetrating networks exhibit ultrafast charge transfer (~40 fs) [6].

Altogether, organic photovoltaics have many attractive features; they are flexible, semitransparent, have the potential to be manufactured in a continuous printing process, have a large area coating and easily integrated in different devices are significantly less expensive than traditional solutions, and have substantial ecological and economic

advantages. These features are beneficial for commercialization; however, organic photovoltaics have to fulfill the basic requirements for renewable energy production. In the present market the competitive position of every technology is mainly determined by efficiency, lifetime and cost ($/W). Figure 2 shows restrictions in commercialization of organic solar cells. The idea of the critical triangle is all the three technology driving aspects should be fulfilled at the same time.

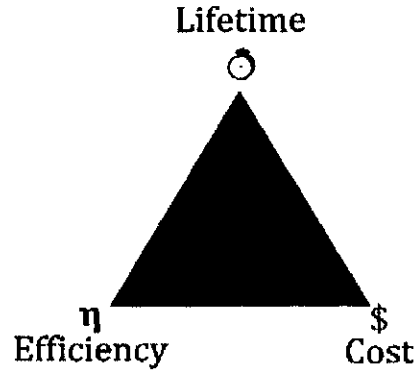

Figure 1.2. Critical triangle for photovoltaics which shows main aspects to be fulfilled to commercialize a product.

To harness the huge amount of energy provided by the sun every second represents the main challenge that the solar photovoltaic technology faces. Starting with the introduction of silicon as the prime semiconductor material used for solar cells in the late 1950s, followed by amorphous silicon a-Si:H in the last years of 1970s, then the thin film technology, CIGS (η = 19.2%) and CdTe (η = 16.7%), now it is the turn of photochemistry and semiconductor physics to make a decisive contribution in this field. The best research cells and their efficiencies tested by National Renewable Energy Laboratories are shown in figure 3. Inorganic PV reach 50% efficiency while the alternative, organic PV, is still below 10%.

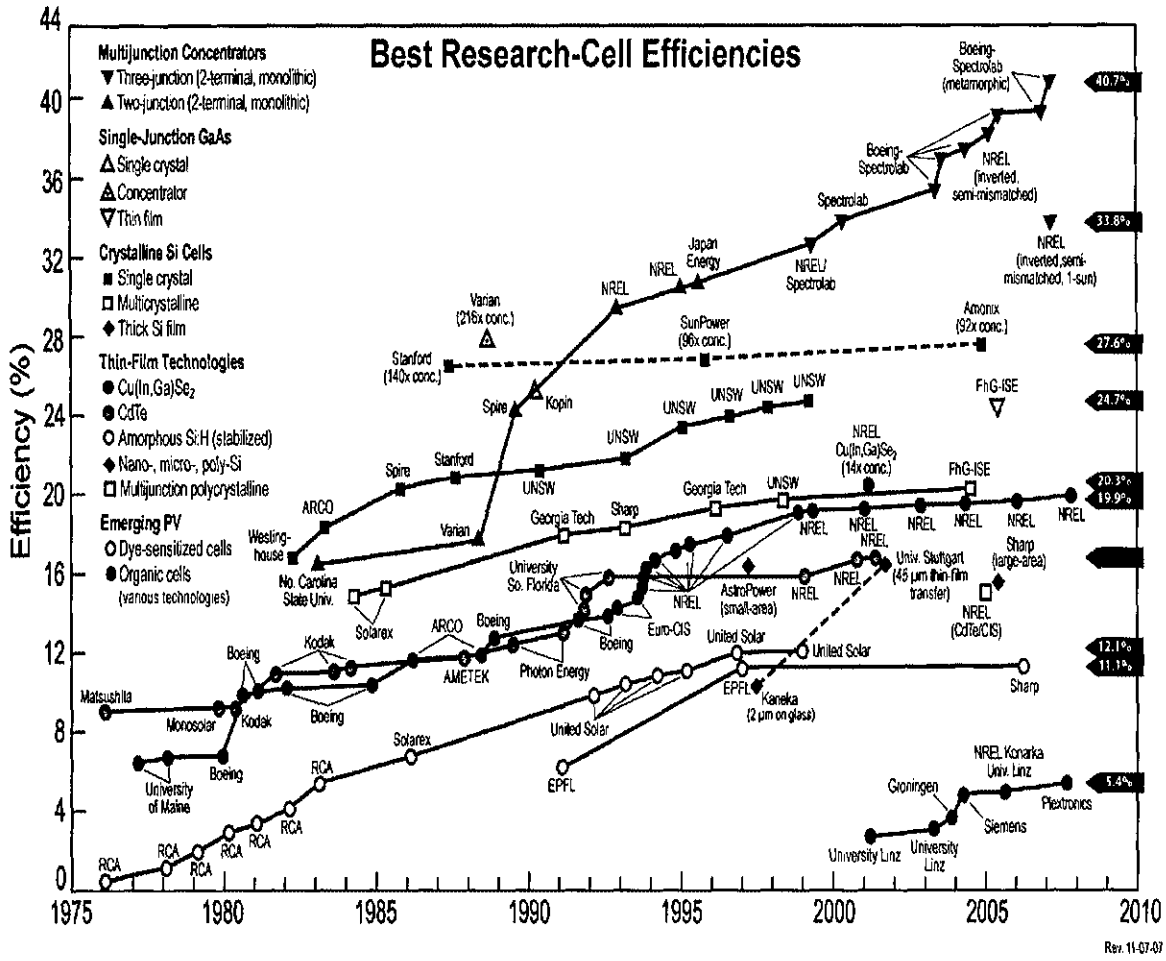

Figure 1.3. Power conversion efficiencies of inorganic and organic laboratory solar cells under AM1.5 Global 1000 W/m^2 illumination [3].

The structure of this thesis work is as follows: Chapter 2 briefly describes physical and chemical properties of conjugated polymers and their composites with fullerenes, configuration and working principle. Chapter 3 provides brief description of materials used in organic solar cells. Chapter 4 describes fabrication of organic solar cells. Chapters 5,6,7 present experimental methods used in investigating and characterization of optical, surface properties using UV-Vis spectroscopy, Spectroscopy Ellipsometry (SE), Atomic Force Microscopy (AFM). Chapter 8 explains interrelation of data obtained from experimental data. Chapter 9 presents performance characteristics. Chapter 10 concludes the thesis work and future prospects given.

CHAPTER II

PHYSICS OF ORGANIC SOLAR CELLS

The conducting and semiconducting properties of polymers were discovered when poly-acetylene, a simple polymer, was accidentally doped with iodine concentrations, which were three orders of magnitude larger than intended [12]. This leads to the invention of several conducting and semiconducting materials. A common structural feature of all these materials is the alternation between single and double bonds between carbon atoms.

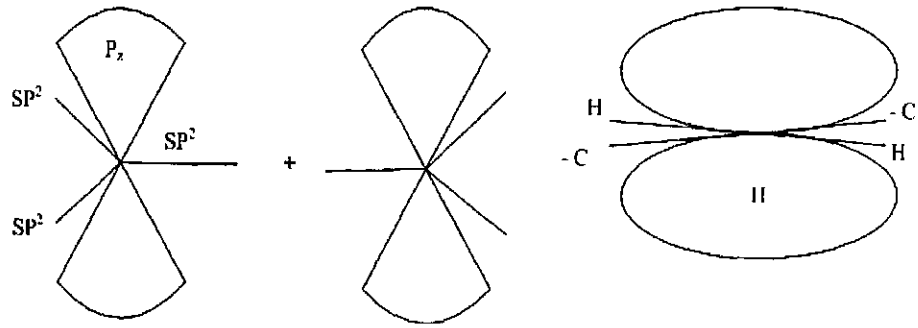

Figure 2.1. Formation of delocalized Π electrons along the polymer chain. Π electrons are contributed from P_z orbital. Semi conducting properties of organic materials are due to repetitive Π bonds.

In the carbon p_z orbital, this is perpendicular to the plane defined by the sigma bonds. The P_z orbital from neighboring carbon atoms overlaps and forms a delocalized Π bond. In the energy model, this would be equivalent to the sigma bonds forming low lying completely filled bands, while the Π bonds lead to an only partially filled band from which the important electronic properties arise. Bonds between neighboring carbon atoms alternate between longer single and shorter double bonds. The consequence is that the Π band splits energetically into two bands, Π and Π* because the unit cell now consists of two CH monomers. One band is completely occupied (HOMO or valence band) and the other completely unoccupied (LUMO or conduction band) respectively, resulting in a 1D intrinsic semiconductor.

The basic steps of photovoltaic conversion in OSC are described below in detail

Incoupling of photons – Typically photovoltaics are manufactured on glass substrates or PET where photon encounters occur. The criterion is that the material should be as transparent as possible for light. The losses due to reflection at the air substrate interface should be minimized. The higher the difference of the optical refractive index at interfaces the higher the losses. Any redirecting of photons from normal incidence to some degree of coplanarity with the film surface will help absorption as the path length increases.

Light (Photon) absorption (η_A) – The active layer is defined as the layer where beneficial absorption takes place. It is important to focus as much energy as possible to this active layer. Optical electrical field (|E|) and absorption are closely related. $|E|^2$ is dependent both on the local dielectric function and on device structure and optical properties of the interface layers. From a material perspective, active material absorption coefficient should match solar irradiation to absorb more photons.

Exciton formation - In conjugated polymers the delocalized p_z orbitals constitute the π bond produce two orbitals: a lower bonding (π) orbital and a higher antibonding (π^*) orbital. Energy gap of the semiconducting polymer material is the difference between two energies of these states. When photons with energies equal to or above the band-gap energy hits material, generates an electron in the π^* level and a hole in the π level due to electron transitions from π-HOMO to π^*-LUMO bands. The generated electron and hole in conductive polymer are loosely bound together by Coulombic force. This electron-hole pair is called exciton, and it moves within the material as a one entity also called as exciton.

Exciton migration - In a diffusive three-dimensional migration the exciton moves through the material. A parameter describing this process is the exciton diffusion length, L_D, Typically it is of the order of 5–10nm but is dependent on the structure of the

materials and the dielectric environment [14]. The generation of an electron–hole pair, by photoexcitation, results in an excited but neutral state with a limited, finite lifetime. This state is termed exciton and consists of an electron and a hole paired by energy (E_{ex}) that is smaller than the energy gap between the limits of the permitted bands (LUMO and HOMO bands, respectively). If E_G is the energy gap, then ($E_G - E_{ex}$) is the exciton binding energy. Exciton during their diffusion they end their existence via recombination. The desired path is the transformation of the excitons into free electrons and holes, which is assumed to happen at certain dissociation sites where two materials with different electron affinities come into proximity of each other. Conditions for generating charge from excited states may also be found in inhomogeneities in materials, and at interfaces to electrodes, but are typically very inefficient compared to processes of photoinduced charge transfer at junctions between two dissimilar materials, and are therefore neglected here. From the diffusion length L_D, we define a diffusion zone. This is the part of the device that has the ability to give charge carriers for a photocurrent.

Exciton dissociation (η_{TC}) - Photo response in OPV cell requires splitting of the excitons before their recombination, that is, within about 10 nm from the site of the light absorption. The excitons can be dissociated by charge transfer at interfaces such as the interface between a metal and the polymer material or interface between molecules of different electron donating and accepting properties. The electron is accepted by material (electron acceptor) with larger electron affinity and the hole by material (electron donor) with lower ionization potential. The excitons can also be dissociated simply in an electric field strong enough to overcome the Coulomb attraction between the electron and the hole in the exciton. In donor-acceptor molecular junctions, the charge separation process can be further separated into an excitonic step, where a sort of charge transfer exciton is formed with an electron in the acceptor side and a hole in the donor side of the junction, and to an electronic step, where the electron and hole are separated by thermal dissociation or ionization in an electric field (Yoshino et al. 1997).

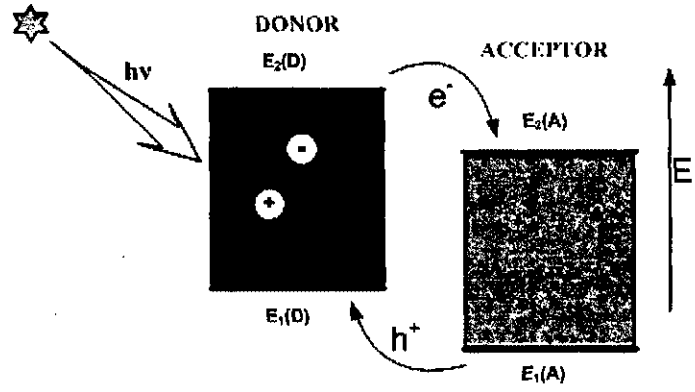

Figure 2.2. The energy levels of a donor-acceptor system. Efficient donor-acceptor separation depends on difference in electron affinity and ionization potential of materials. Charge transfer of OSC materials is very fast <45fs for a combination [13]

Exciton diffusion (η_{diff}) – This quasi particle diffuses inside the donor material as long as recombination processes do not take place. Forster (long range) or Dexter (between adjacent molecules) transfers can take place between an excited molecule (excitation donor) and a molecule that receives the excitation (excitation acceptor).

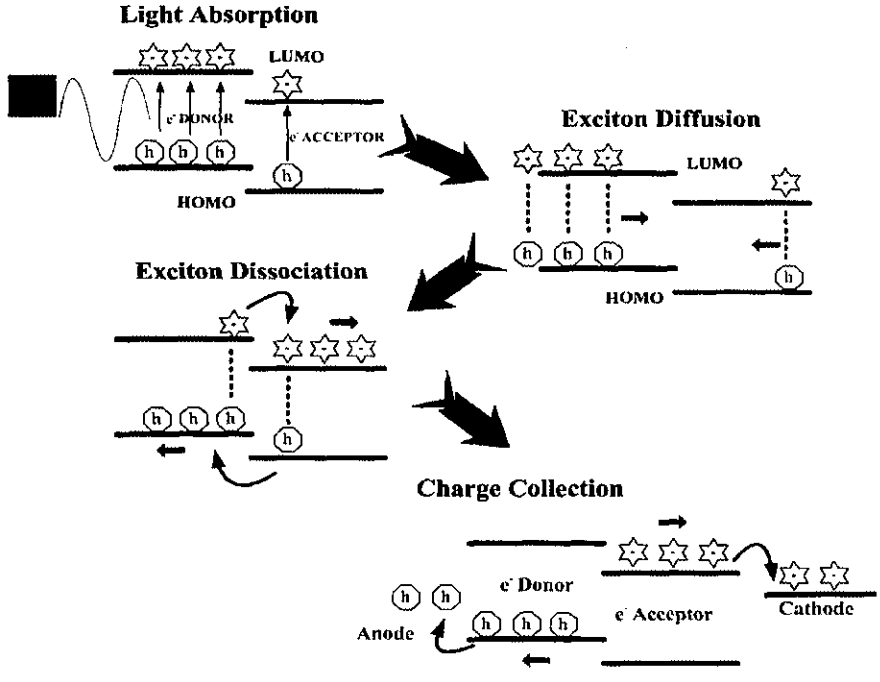

Figure 2.3. The basic steps of photovoltaic conversion in OSC including 1.Light absorption, 2.Exciton diffusion, 3.Exciton dissociation 4.Charge transport and collection.

Carrier transport (η_{tr}) – this transport involves the classic mechanism for hopping processes in organic materials.

$$(E_F)_{cathode} < (E_{LUMO})_{acceptor} \text{ and } (E_F)_{anode} > (E_{HOMO})_{donor}$$

Where $(E_F)_{cathode}$, $(E_F)_{anode}$ are work potentials (eV) of cathode and anode respectively

Charge collection - separated electrons and holes are transported to the opposite electrodes in an internal electric field created by asymmetry of the electrodes (different work functions) or in built in potentials (Yoshino et al. 1997). In order to reduce recombination, the electrons and holes are preferentially transported in different materials or phases. For example an acceptor material with good electron conductivity and a donor material with good hole conductivity is ideal. Good non blocking contacts between the molecular materials and the electrodes are essential for efficient charge collection. In some cases an additional material layer may be needed between the metal and organic layer to facilitate good ohmic contact, such as LiF between P3HT-PCBM blend and aluminum (Shaheen et al. 2001a, Brabec et al. 2001b).

CHAPTER III

MATERIALS

This chapter gives details about materials used in processing OSC. Indium tin oxide (ITO) acts as a transparent conducting electrode, fullerenes derivatives as electron acceptor, semiconducting polymer materials as electron donors, PEDOT:PSS as buffer layer and chlorobenzene as solvent to mix active layer are described. Properties and the absorption spectrum under standard operating conditions are also shown.

3.1 ITO

Indium tin oxide is a mixture of 90% indium (III) oxide (In2O3) and 10% tin (IV) oxide (SnO2) by weight. ITO is used to make Transparent Conducting Oxide (TCO) coatings in Organic photovoltaics and Light Emitting Diodes. The main feature of ITO is to provide combination of electrical conductivity and optical transparency at the same time. A high concentration of charge carriers will increase the materials conductivity. These carriers are free electron and oxygen vacancies and an excessive population produces absorption [15]. High conductivity or low sheet resistance is balanced against high transmission in the visible region.

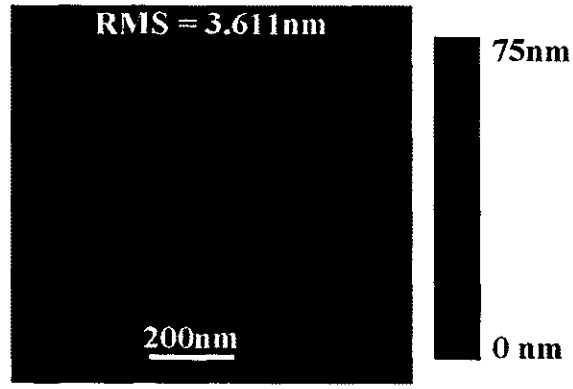

Figure 3.1. Surface topography of Indium Tin Oxide after cleaning.

Sheet resistance can be less than 10 Ω/sq with a visible transmission of >80%. To obtain transmission near 90%, sheet resistance must be >100 Ω/sq. ITO films behave as metals to long wavelength light because of the presence of a plasma wavelength above 1 μm. At

longer wavelengths, the film becomes reflecting. The refractive index for transparent film in the visible region remains near 1.95 and is not strongly dependent on the deposition parameters. Index is generally of secondary concern for conducting applications. The extinction coefficient will vary with conductance.

3.2 Fullerene Derivatives

Carbon fullerenes are large, closed cage carbon structures in a spherical shape. Fig 1. represents C_{60} fullerene molecule. A fullerene is a spherical structure composed of both pentagonal and hexagonal carbon rings. Fullerenes are considered zero dimensional quantum structures that exhibit interesting quantum properties. C_{60} or buckminsterfullerene is an electron acceptor.

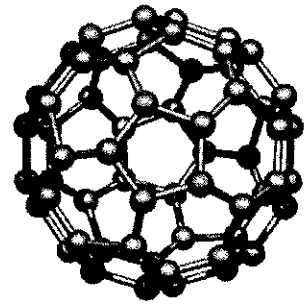

Figure 3.2. C_{60} Fullerene molecule showing hexagonal and pentagonal bonds of carbon atom.

C_{60} itself is rather insoluble, which is a major drawback. The lack of miscibility between the p-conjugated polymer and C_{60} resulting in phase segregation and clustering of the fullerene component, thus decreasing the donor–acceptor electronic interaction as well as the charge transport of the photogenerated electrons and holes. Side groups are attached to increase its solubility for the application in solution-cast processes. Therefore, a soluble derivative called PCBM [(1-(3-methoxycarbonyl) propyl-1-phenyl [6,6]C_{61})] [21][22] is used with C_{60} in solar cell devices. The structure of PCBM is shown in figure 3.2. Methanofullerene Phenyl-C_{61}-Butyric-acid-Methyl-ester (PCBM-C_{60}) is an effective solution processable n-type organic semiconductor. PCBM-C_{60} is the most commonly

used n-type semiconductor in organic photovoltaics (OPVs) [16]. This methanofullerene derivative is quite robust compound, highly soluble in aromatic hydrocarbons like chlorobenzene. Fabrication of thin film organic electronics devices is complex, with slight variations of molecular structures having profound effects on film morphology and charge transport. Chemical alterations of the C_{60} molecule by adding side chains increase its solubility and electronic properties. The size and dispersion of the PCBM nanophases have a direct impact on the device performance. PCBM-C_{70} is mixture of isomers and shows better absorption spectrum in visible region.

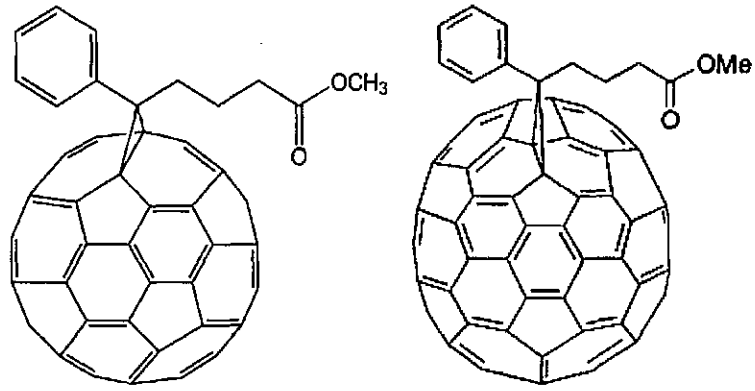

Figure 3.3. Chemical structure of PCBM-C_{60}, PCBM-C_{70}.

3.3 Conjugated Polymers

Poly (3-hexylthiophene), particularly π-conjugated poly (3-hexylthiophene) (P3HT), has been of interest because of high carrier mobility, mechanical strength, thermal stability and compatibility with the fabrication process. Advances in synthesis of regioregular polyalkylthiophenes (PAT) have significantly improved the electronic properties by increasing conjugation length. The regular head to tail arrangements of the alkyl side chains in regioregular PATs has improved the crystalline coherence length over that in the regiorandom PATs. Conductivity increases upon increasing the length of side chain from butyl to decyl. The maximum conductivities obtained for various regioregular PATs are found to be maximized for P3HT. [Handbook of Conducting Polymers]

Regioregular means that the alkyl side chains of the P3HT are aligned in a periodic structure as opposed to the regiorandom case. Polythiophene is the actual conjugated polymer backbone, and the rest are side chains. The function of side chains is to make materials soluble in organic solvents like chlorobenzene, toluene and chloroform. An additional function of side chains is to modify electro-optical properties of the materials. Morphology can also be influenced by the regularity of the side chains.

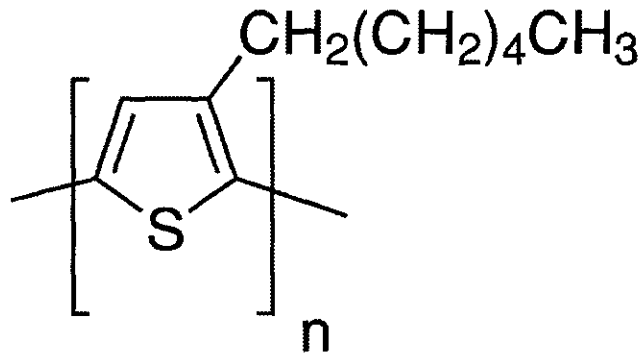

Figure 3.4. Structure of P3HT [Poly (3-hexylthiophene)].

Standard absorption spectrum of thin film of pristine P3HT spun from chlorobenzene (1:1wt%) is shown and peaks are indicated.

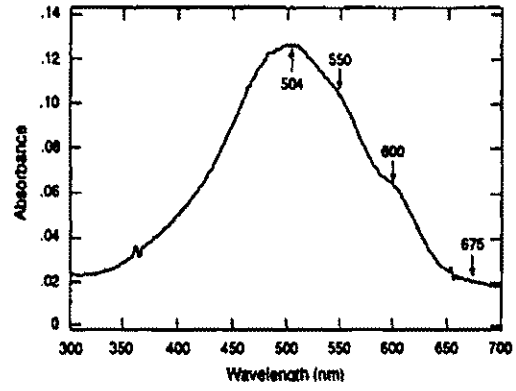

Figure 3.5. Absorption spectra of P3HT thin film.

3.4 PEDOT:PSS

Poly(3,4-ethylenedioxythiophene) [PEDOT] belongs to the class of semiconducting polythiophene and was developed during a search for stable conducting polymers. Introduction of the dioxyethylene substitution circumvents undesired (α, β) and (β, β) coupling of the thiophene ring and leads to air stable material in its doped oxidized form due to its electron rich character (low oxidation potential) [17]. PEDOT has relatively high conductivity in its oxidized form which can be ascribed to a planar structure allowing effective delocalization of Π electrons. Conjugated polymer PEDOT has a unique combination of properties that make it extremely attractive for organic electronics applications. It is used as charge injecting layer as well as electrodes in photovoltaic cells.

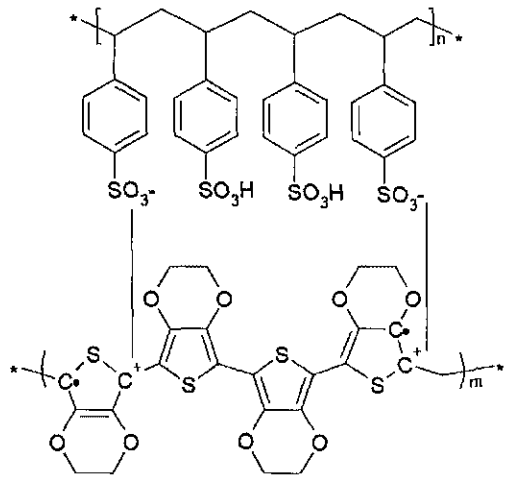

Figure 3.5. Chemical structure of PEDOT:PSS

PEDOT has good optical transparency in the visible region but it is an intrinsically insoluble polymer that can be chemically or electrochemically doped. Doping changes PEDOT from an opaque insulator to a quasi transparent material with high electrical conductivity. Poly (Styrene Sulphonate) resolved this problem. PSS acts as charge compensating counter-ion to stabilize the p-doped conducting polymer, and forms a processable water-borne dispersion of negatively charged swollen colloidal particles consisting of PEDOT and excess PSS [26]. PEDOT and PSS chains are linked tightly by ionic interactions and form an ionic polymer complex that can be soluble in water.

Commercial materials supplied by H.C.Stark have a conductivity of about 10^{-3} S/cm [27]. The actual conductivity strongly depends on morphology of dried particles in the film that depends on annealing conditions [17] and on the distribution of PEDOT segments in the matrix. For PV devices, PEDOT:PSS serves following advantages

1) It prevents a device from being shorted, since most of OSC are bulk heterojunction structures and there is always the unavoidable chance of current leakage. PEDOT:PSS blocks the electrons leaking through ITO (anode).
2) PEDOT:PSS wok function is 0.2 – 0.3V higher than ITO, which helps to have an ohmic contact between ITO and active material that improves open circuit voltage.
3) PEDOT:PSS is also known to help adhesion of photoactive layer to ITO thus decrease the series resistance of the device.

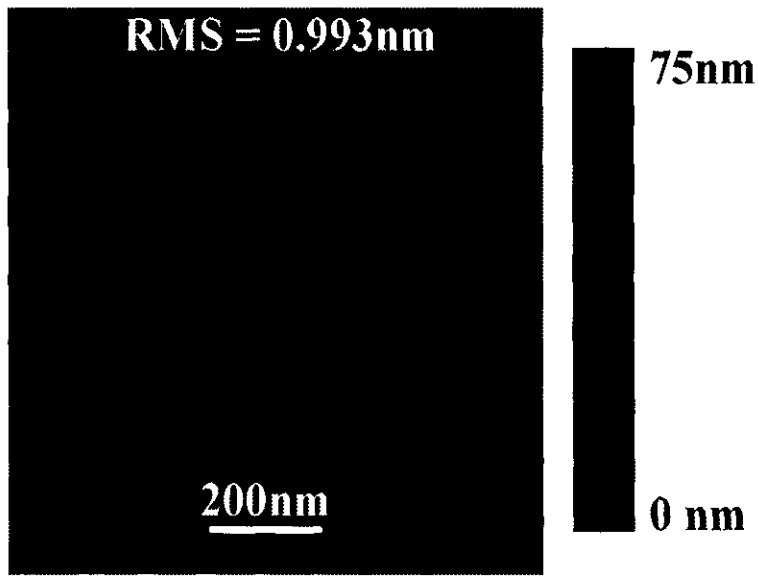

Figure 3.6. Surface topography of Indium Tin Oxide after spin coating with PEDOT:PSS and dried in nitrogen atmosphere at 150^0C for 30 min.

3.5 The Metal Cathode

The cathode is typically realized by vacuum deposition of a low work function metal through evaporation on the organic absorber layer. A thin layer of aluminum is the most common cathode, but other materials have been tested, e.g. LiF/Al, Ag/Al.

3.6 Organic Solvents

Chlorobenzene (CB) is a colorless, flammable liquid. Some of it will dissolve in water, but it readily evaporates into air. It does not occur naturally in environment. Better results are obtained when used to prepare solutions when compared to DCB, Toluene and Chloroform. The slower evaporation of DCB allows P3HT to segregate towards the underlying PEDOT:PSS layer, while the fast loss of CB leads to a more homogeneous blend. Hence, solutions with fast evaporating solvents like chlorobenzene are used to mix conducting polymers with fullerene derivatives.

Table 3.1. Properties of chlorobenzene.

1	**Description**	Colorless, neutral liquid
2	**Molecular formula**	C_6H_5Cl
3	**Molecular weight**	112.56 g/mol
4	**Boiling point**	132^0C
5	**Solubility**	Practically insoluble in water (0.049 g/100 ml); Soluble in alcohol, benzene, chloroform, diethyl ether.

CHAPTER IV

ORGANIC SOLAR CELL PROCESSING

Organic thin film PV devices are fabricated in a sandwiched structure as shown in figure 4.1. This chapter gives a brief description of OSC processing at the laboratory scale. Each production step is described in detail, because of the interdependence between OSC production and OSC properties obtained during characterization.

4.1 Standard OSC structure

Layered structure of OSC is shown in figure 4.1.

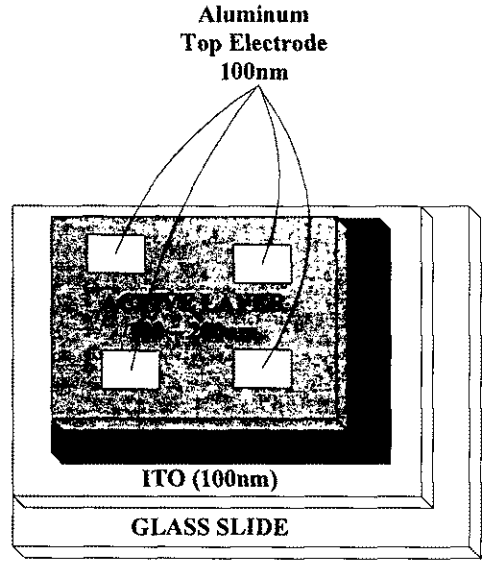

Figure 4.1. Layered structure of organic solar cell with layers of microscopic glass slide, ITO, PEDOT:PSS, Active layer consisting P3HT & PCBM, Aluminum electrode (Bottom to top) and their respective thickness.

In OSC the first layer is Indium tin oxide (ITO) which is used as a transparent conducting oxide (TCO) coated on microscopic glass slide of thickness 1mm. This ITO layers is used as electrode, on top of ITO a thin transparent layer PEDOT:PSS is spin coated, which acts as good hole transporter [23] in OSC. Active layer is spin coated on thin PEDOT:PSS layer, which is a mixture of polymer P3HT (poly(3-hexylthiophene)) acts as donor and PCBM, which acts as acceptor in the ratio 1:1.

4.2 OSC Processing

OSC processing includes several steps including substrate preparation, etching, cleaning, solution preparation, spin coating, annealing and evaporation of electrode.

4.2.1 Substrate Preparation (Etching & Cleaning)

ITO coated substrates are more commonly used electrodes for photovoltaic or Light Emitting Electrode (LED). They are transparent conducting substrates and have transmissions ranging between 90% to 75% depending on conductivity of substrate. A 1" X 1" ITO coated glass slides with sheet resistance less than 15Ω/■ is structured by using polyamide tape as shown in Fig.2.

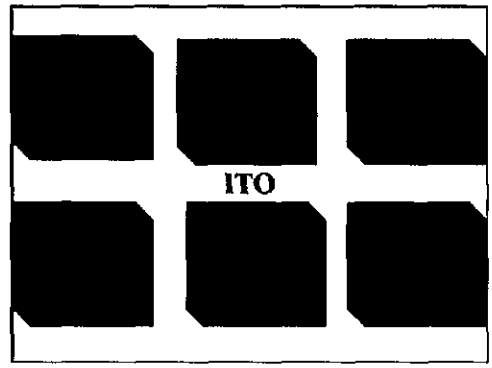

Figure 4.2. 1X1" ITO coated substrate structured using polyimide tape into six blocks prior to etching.

ITO substrates are etched using HCl+HNO_3 mixture. Structured samples are placed 1 minute in HCl:HNO_3:DIwater (1:1:2) mixture to obtain required patterning. Patterned samples are thoroughly cleaned with detergent to remove dust from structuring, and storing. This process is followed by cleaning in a bath sonication with Toluene, Acetone, Isopropanol and DI water for 10 minutes. Samples are immediately dried by blowing with a nitrogen gun. Clean ITO substrates are now ready for OSC preparation. Cleaning is the essential part because cells are much thinner. Small contamination would show a negative effect, which introduces inhomogeneities in thin layers.

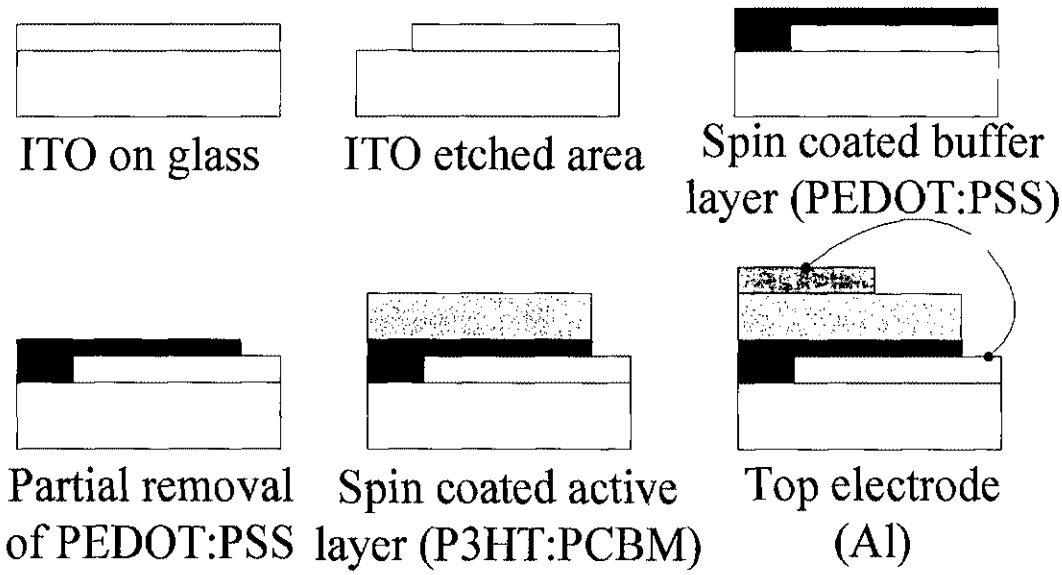

Figure 4.3. Preparation steps for organic solar cell fabrication stepwise [28]

4.2.2 Solution preparation

The second main preparation step is to prepare solutions to be used for spin coating. Two solutions are to be prepared for OSC. One is PEDOT:PSS, and the another solution is mixture of a semiconducting polymer and PCBM, which acts as photoactive blend layer. PEDOT:PSS is available from H.C.Starck. This is used as a hole extraction layer and on top of ITO. For OSCs PEDOT:PSS (type) is used as received and only filtered through 0.45μm filter prior to spin coating. Electron donating polymer P3HT from Rieke Metals, electron acceptor PCBM from Solenne BV are bought and stored in dark in nitrogen glove box where O_2, H_20 ppm levels are less than 0.1. Choice of solvents and concentration affects absorption properties [24] of OSCs [25]. 10mg of P3HT, PCBM are mixed in 1:1 ratio and mixed with 1ml of chlorobenzene. Stir and heat solution to 40^0C, and leave in nitrogen glove box over night till the solution becomes clear and grains are completely dissolved. The filtering step is necessary to reduce impurities in solution otherwise inhomogeneities in active layer during spin coating makes device short circuited. Use 0.45μm filter to take out grains.

4.2.3 Spin coating

There are so many techniques for applying thin films [33] but spin coating [32] is considered to be the most common and easiest process. Substrates are held by vacuum

while supplying N_2 gas. Spin coater spin is slowly increased so that thin films will be spread uniformly. Solvents evaporate by the end of spin coating. Disadvantage of this method are high volume loss of solution and limitation in substrate size.

PEDOT:PSS is spin coated onto ITO substrate in N_2 glove box. Spin at 3000rpm for 80s. Resulting layer can be measured using Atomic Force Microscope (AFM). Spin coating of P3HT+PCBM mixture is carried inside nitrogen glovebox. After spin coating PEDOT:PSS, active layer is spin coated below 2000rpm for more than 120s so the active layer will be dried when we take out sample from spin coater.

4.2.4 Annealing

Annealing is a process of drying at elevated temperatures to take out solvent content from thin films.

PEDOT:PSS drying

PEDOT:PSS thin films are annealed above 100^0C for less than an hour to take away any residual H_20 content. This process increases PEDOT:PSS film's conductivity as well as crystallinity.

Table 4.1. Parameters for spin coating of PEDOT:PSS, Active layer and drying conditions for both layers.

PARAMETER	PEDOT:PSS LAYER	ACTIVE LAYER
Ramp Speed	1000rpm	100rpm
Speed	4000rpm	800 – 2000rpm
Spin Duration	80s	120s
Annealing Temperature	>100^0C	Ambient
Annealing Duration	10min – 1hour	-
Atmosphere	Vacuum	Nitrogen glovebox
Pressure	<600mbar	<6mbar

4.2.5 Evaporation of Cathode

E-beam deposition is used to deposit an aluminum cathode. In evaporation the substrate is placed inside a vacuum chamber, in which the graphite crucible is filled with aluminum pellets are also placed. The source material is then heated until it starts evaporating. During deposition pressure is maintained below $5*10^{-6}$ mbar to allow molecules to evaporate freely in the chamber, and they subsequently condense on all surfaces uniformly. In e-beam electron beam is bent in such a way that it is aimed at the source material causing local heating and evaporation. Layer thickness is monitored by an oscillating crystal. Al cathode deposited for 100nm in standard case. The schematic of an diagram of e-beam working is shown in figure 4.4.

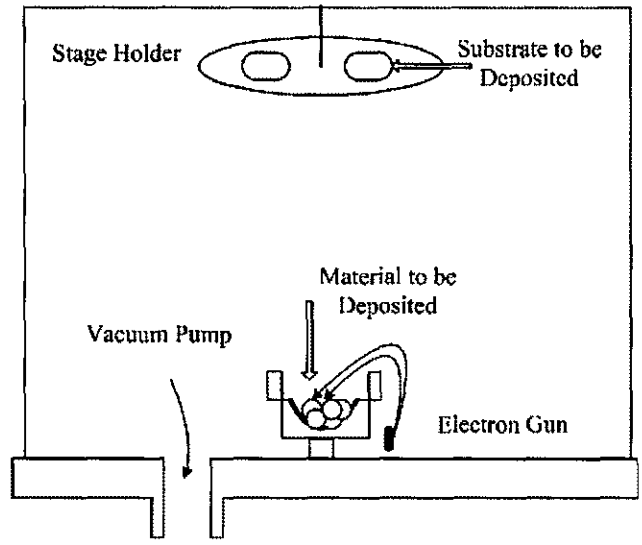

Figure 4.4. Schematic representation of electrode evaporation using E-beam technique.

4.2.6 OSC Post-Treatment

Post treatment of OSC is a critical step for its performance. When fast evaporating solvents like chlorobenzene, dichlorobenzene are used post treatment improves the OSC efficiency dramatically. Post treatment induces increased absorption as well as better mobility of charge carriers and improvement of the contacts. Post treatment is performed

on temperature controlled hotplate inside nitrogen glovebox. Complete processing steps of OSC are shown below in a schematic way.

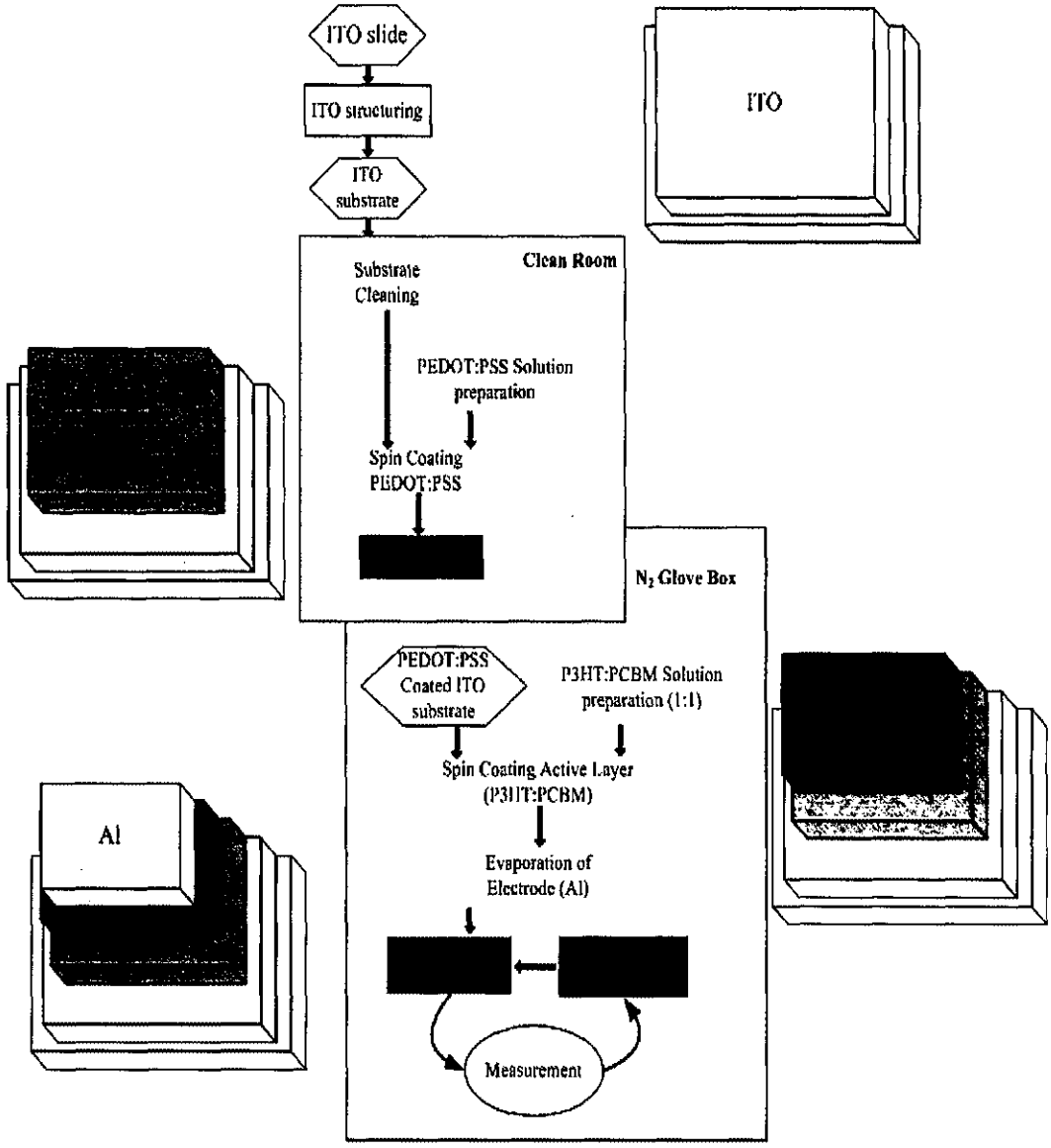

Figure 4.5. Illustrated production process of OSC step by step where left, right side shows layered structure and middle shows processing sequence.

CHAPTER V
UV VISIBLE SPECTROSCOPY

An electronic transition occurs from HOMO to LUMO in molecules when samples are exposed to light having an energy that matches a possible electronic excitation. Some of the light energy will be absorbed when an electron is promoted to higher energy orbital. Different molecules absorb radiation of different wavelengths. An absorption spectrum will show a number of absorption bands corresponding to structural groups within the molecule. The appearance of several absorption peaks or shoulders for a given material is common for a highly conjugated polymer.

The visible and UV region of the spectrum comprises photon energies of 1.65 to 3.1eV and 3.1 to 124ev respectively. These energies are sufficient to excite a molecular electron to a higher energy orbital. There are various kinds of electronic excitations which occur in molecules as shown in figure 5.1. Most absorption spectroscopy of organic compounds is based on transitions of n or p electrons to the p* excited state. This is because organic compounds with high degree of conjugation absorb light in UV or visible regions of EM spectrum.

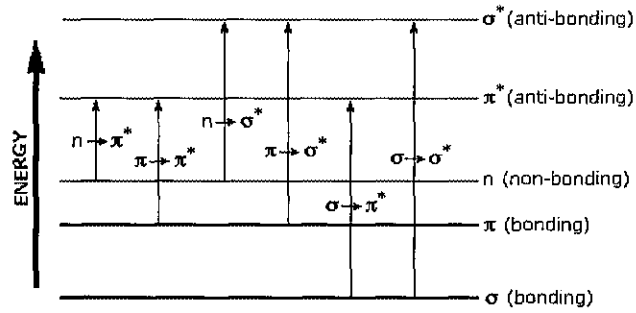

Figure 5.1. Different types of electronic transition in molecules when exposed to light spectrum. UV and visible spectrum consists of photon energy which favors excitation from one states to other states.

A perkin Elmer Lambda 2S UV/Vis spectrophotometer was used for transmission and absorbance studies on thin films. A D2 lamp and a tungsten (W) lamp were used as

UV and visible wavelength sources respectively to provide spectrum from 250nm to 750nm. General spectrophotometer schematic is shown in figure 5.2. The light source from both lamps is split into two equal beams by using diffraction grating and mirror setup. These two beams are passed through reference and standard sample and intensity at the end was measured to determine the absorption spectrum of sample.

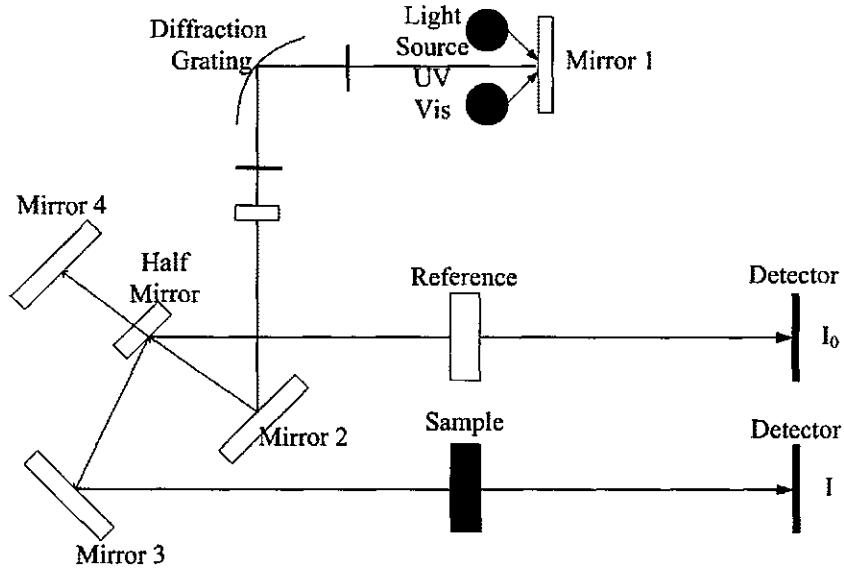

Figure 5.2. Typical spectrophotometer components 1) Light source, 2) Diffraction grating, 3) Equal beam split half mirror device, 4) Sample holders, 5) Detector.

ITO samples were analyzed perpendicular to the incident beam in transmission mode. After determining transmission spectra of ITO slides, PEDOT:PSS films are coated and again transmission spectra were determined. Absorption spectra of pristine P3HT, PCBM-C_{60}, PCBM-C_{70}, P3HT:PCBM-C_{60} and P3HT:PCBM-C_{70} mixtures were also investigated before and after thermal annealing. All organic thin films were measured in absorption mode on glass substrates and subsequently corrected for substrate absorption. The absorption spectra of pristine material shows a higher peak around 500-550 nm but for the absorption spectra of the blends (Figure 5.4) clearly show two peaks: one around 340 nm corresponding to the PCBM, while the other peak is in the region

500-550 nm represents the contribution of the P3HT. The latter shows a pronounced red-shift upon thermal annealing, while the peak of PCBM remains unchanged [29][30].

Table 5.1. Describes how the maximum absorption spreads over wavelength as the annealing temperature increases.

ANNEALING TEMPERATURE (^{0}C)	MAXIMUM ABSORPTION SPREAD OVER WAVELENGTH
Unannealed	526 – 527
60^{0}C	527 – 528
70^{0}C	526 – 529
90^{0}C	521 – 530
110^{0}C	520 – 530
130^{0}C	525 – 527
150^{0}C	520 – 530

The degree of inter chain and intra chain ordering in films of P3HT can be judged from their optical absorption spectra. Below figure 5.3 shows enhanced shoulders around 610nm upon annealing P3HT thin films at elevated temperatures. For annealing temperatures below 100^{0}C the absorption spectrum doesn't seem to change much.

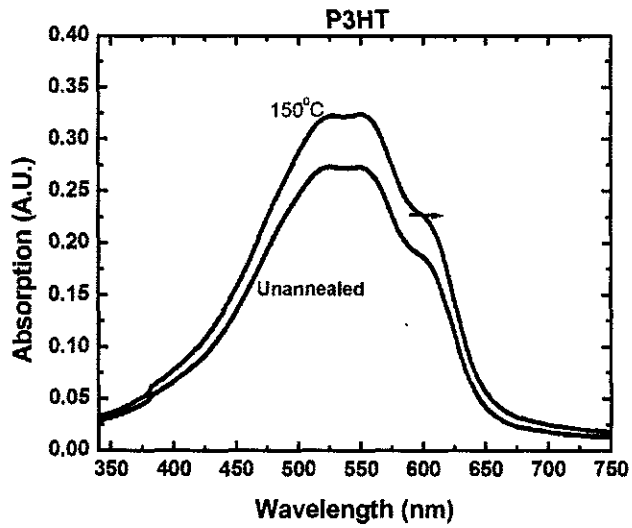

Figure 5.3. Red shift of pristine P3HT films spun from chlorobenzene and enhanced shoulder upon annealing at elevated temperatues.

Films of higher ordering display a redshifted π-π* absorption band with more pronounced vibrational structure [35]. The greater the degree of conjugation [36] (adjacent sp^2 hybridized atoms) the larger the shift of λ_{max} towards longer wavelength values. The maximum absorption spread shows red shift upon annealing at higher temperatures.

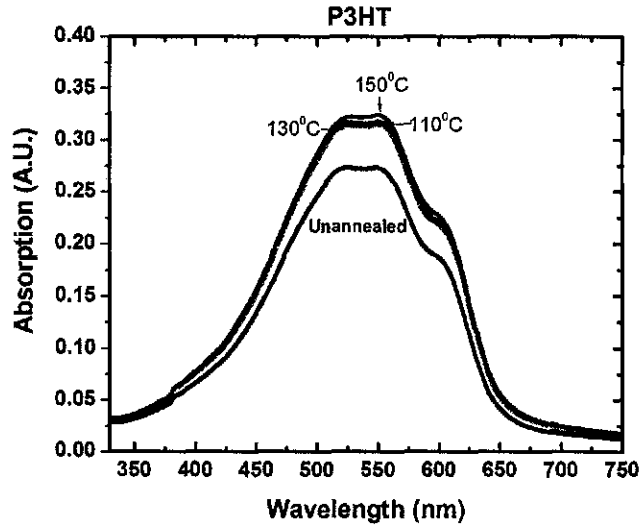

Figure 5.4. UV-Vis absorption spectra of pristine P3HT films, as-cast, unannealed and annealed above 100^0C for 10 minutes inside nitrogen glove box with ppm levels below 0.1ppm. Films were spin cast in chlorobenzene (1:1wt %). All films were measured on glass substrate and corrected for substrate absorption.

The analysis of the natural bond orbital (NBO) suggested that there were about 0.11 electrons transferred from the moiety phenyl and butyric acid methyl group of PCBM to fullerene cage [39]. Absorption bands of PCBM are located in the UV region. The calculated absorption bands near 349nm agreed well with the experimental measurements. UV-Vis spectra of PCBM measured in chlorobenzene solution are found to have absorption bands centered at 282nm and 336nm. Due to disturbance in near UV region we could not find peaks below 300nm using lambda 2S spectrophotometer. Absorption in visible region is much weaker than the UV region. The main absorption bands of C_{60} are always below 400nm. Thus, the weak absorption bands above 400nm

may be related to the ligand to fullerene cage charge transfer process. Figure 5.5 shows uv-vis spectrum of PCBM-C_{60}.

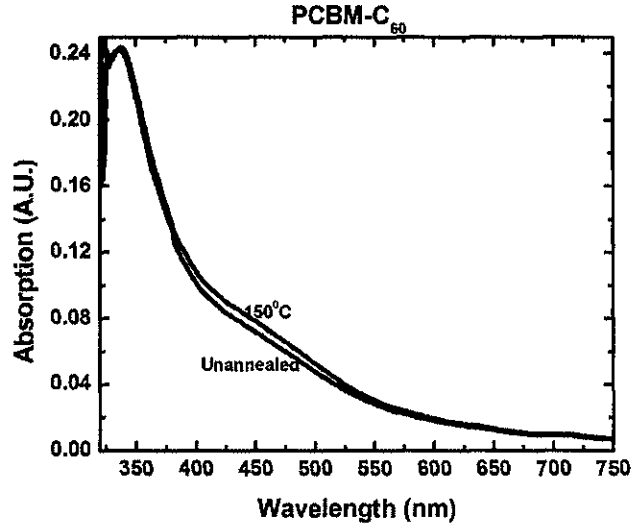

Figure 5.5. UV-Vis absorption spectra of pristine PCBM-C_{60} films spun cast from chlorobenzene (1:1 wt %). Samples are annealed for 10 minutes.

Figure 5.6 shows uv-vis spectrum of PCBM-C_{70}. Unlike PCBM-C_{60}, PCBMC_{70} has absorption peaks in the visible region also.

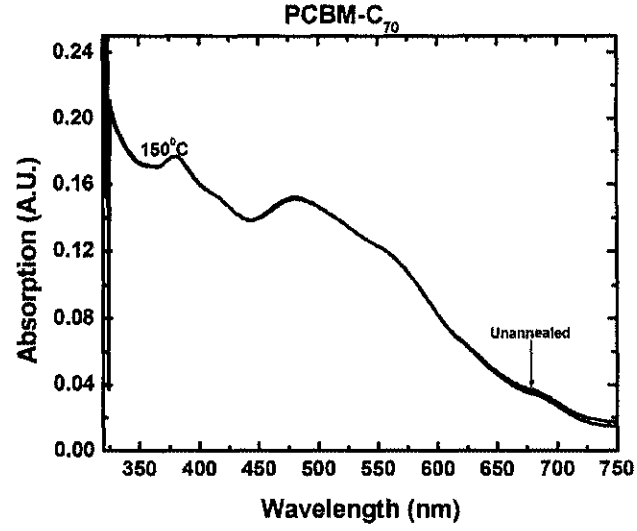

Figure 5.6. UV-Vis absorption spectra of pristine PCBM-C_{70} films spun cast from chlorobenzene and annealed for 10 minutes. All films were measured on glass substrate and corrected for substrate absorption.

No enhancement in the absorption spectrum was observed for PCBM films even though samples annealed at elevated temperatures. From these absorption measurements we can conclude that films made of PCBM are not crystalline. UV-Vis spectrum for PCBM-C_{70} compared with its analogous PCBM-C_{70}. Distinct peaks for both films were observed at different wavelengths. PCBM-C_{70} has broader absorption spectrum and visible absorption peaks which favors more charge generation in photovoltaic cells.

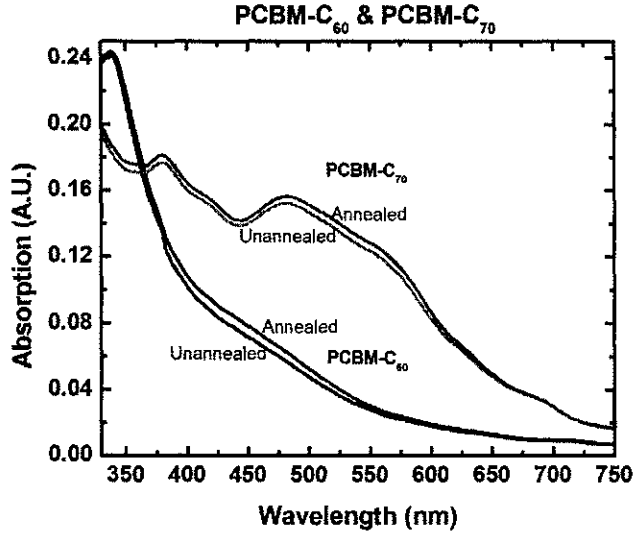

Figure 5.7. Comparison of absorption spectra for PCBM-C_{70} and its analogues PCBM-C_{60}.

Absorption of P3HT:PCBM composite films at elevated annealing temperatures show intrinsic peaks owing to P3HT itself develop distinctly with the heat treatment in a certain range. Thermal annealing increases interdiffusion and mutual mixing of P3HT and PCBM. Mixing of acceptor and donor materials properly results in improved charge transport and device performance [38][39]. PCBM diffuses out of the polymer matrix to form percolated paths up on annealing the P3HT:PCBM composite film, resulting in an increase in the carrier mobility in the active layer. Phase segregation between P3HT and PCBM also took place upon heat treatment [37]. Figure 5.8 shows absorption spectrum of P3HT:PCBM-C_{60}. Upon thermal annealing highly ordered films are obtained as well as conjugation lengths are increased which enhances side chains as well as shifted towards longer wavelength regions (red shift).

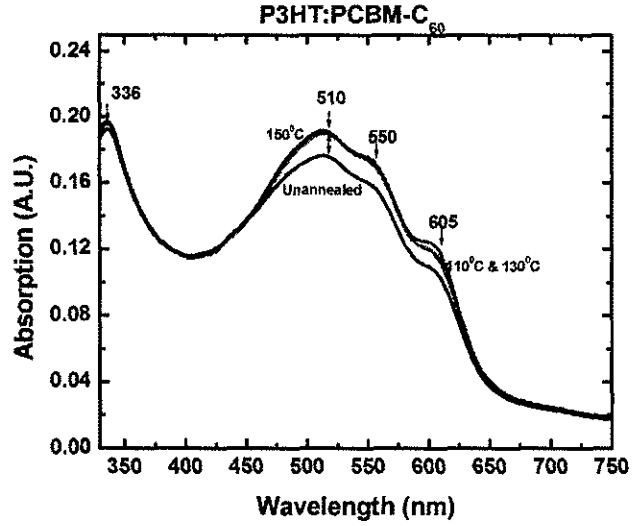

Figure 5.8. UV-Vis absorbance spectra of P3HT:PCBM-C_{60} films, as-cast, and for different annealing temperatures for 10 minutes. Films are spin cast in chlorobenzene (1:1 wt%). All films were measured on glass substrate and corrected for substrate absorption.

Due to absorption peaks in the visible region for PCBM-C_{70} the absorption for P3HT:PCBM-C_{70} peaks out in visible region when compared to P3HT:PCBM-C_{60}. Figure 5.9 shows uv-vis spectrum at different annealing temperatures, and comparison of uv-vis for composite films are shown in figure 5.10.

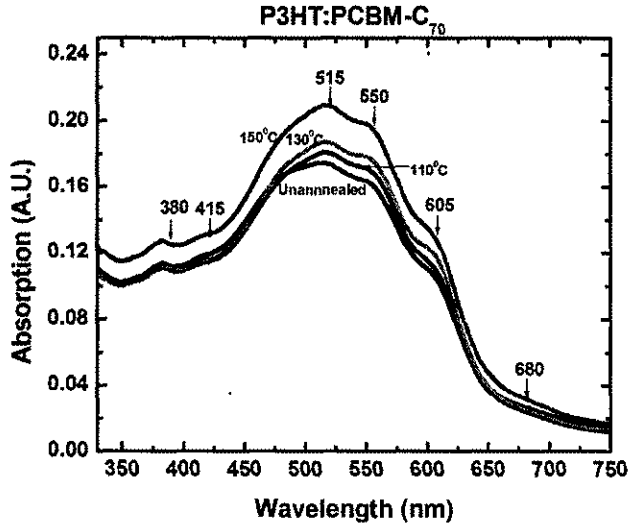

Figure 5.9. UV-Vis absorbance spectra of pristine P3HT:PCBM-C_{70} films, as-cast, and for different annealing temperatures.

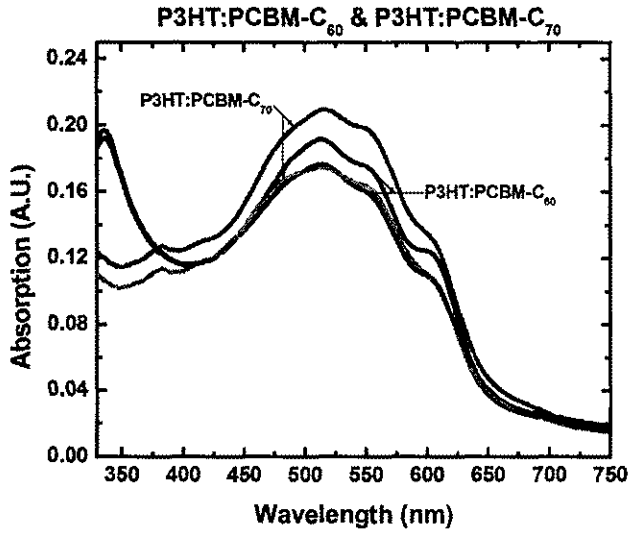

Figure 5.10. Absorption spectra comparison for P3HT:PCBM-C_{60} and P3HT:PCBM-C_{70}.

Absorption maxima of P3HT:PCBM-C_{60} and P3HT:PCBM-C_{70} are compared below for films annealed above 100^0C at λ = 514nm.

Table 5.2. Comparison of absorption values for P3HT:PCBM-C_{60} & P3HT:PCBM-C_{70}

Annealing Temperature (^{0}C)	Unannealed	110	130	150
Max. Absorption P3HT:PCBM-C_{60}	0.187	0.195	0.2	0.204
Maxi. Absorption P3HT:PCBM-C_{70}	0.21	0.245	0.241	0.248

The absorption measurements, correlated with the morphology investigations [3-6] pointed out that there is a change in the physical conformation of the P3HT chains upon annealing at elevated temperatures. As a result, the packing of P3HT together in the presence of PCBM relative to pristine P3HT films changes, thereby adapting the relevant optical and electronic properties that are critical for the operation of these devices. This change in the conformation is also reflected in the absorption spectra of the blend films. Upon annealing, curves shift towards lower photon energies. This shift might originate from a tighter chain coil, produced by twisting the polymer backbone or broken conjugation in the presence of PCBM, resulting in segments with a shorter conjugation length and weaker interchain interaction. This is in agreement with absorption spectra of

pristine P3HT, which show not much change after annealing. Rather, they show a small increase in the absorption intensity. Upon annealing, the PCBM demixes from the P3HT, as inferred by Yang et al. [31], thereby increasing the degree of crystallinity of the polymer and consequently undergoes a noticeable red shift, approaching the spectrum of the pristine polymer. It appears (from figure 5.4) that the shift of the optical absorption is maximized when the devices are annealed above 100^0C, which closely corresponds with the temperature at which the hole mobility in the blend begins to approach that of pristine polymer. Nevertheless, the net effect of the red-shift of the optical absorption upon annealing, with respect to the non-treated film, is that it will improve the spectral overlap with solar emission, resulting in an increased absorption in the device. The absorption shown in figure 5.8 can be used to estimate the amount of additionally absorbed photons upon thermally annealing the P3HT:PCBM BHJ solar cell.

CHAPTER VI

SPECTROSCOPIC ELLIPSOMETRY

Spectroscopic ellipsometry (SE) is a non-contact, non-destructive optical technique that enables the determination of material refractive indices and layer thicknesses by measuring the change in polarization of a probing light beam upon reflection from a sample. When linearly polarized light reflects from a surface, elliptically polarized light is generated. The amount of induced ellipticity depends on surface properties like refractive index or bulk or layered sample. Ellipsometry technique measures the phase and amplitude relationships between two orthogonal polarizations (p and s waves) upon reflection. When p and s waves are reflected, they experience a phase shift and an amplitude reduction. The ellipsometric parameter Delta (Δ) is defined as d_1 - d_2 where d_1 and d_2 denote the induced phase shift difference between p and s waves, respectively while the ellipsometric parameter tan(Ψ) is defined as the ratio of the complex amplitude of the total reflection coefficient of the p and s waves ($|R_P| / |R_S|$).

Ellipsometry is said to be self-referencing because measurements do not require any reference sample and are largely insensitive to variations in the beam intensity and ambient environment, making this technique highly accurate and reproducible. The data is measured over the entire wavelength range and compared to a mathematically generated model to obtain film thickness and refractive index and dielectric function, etc.

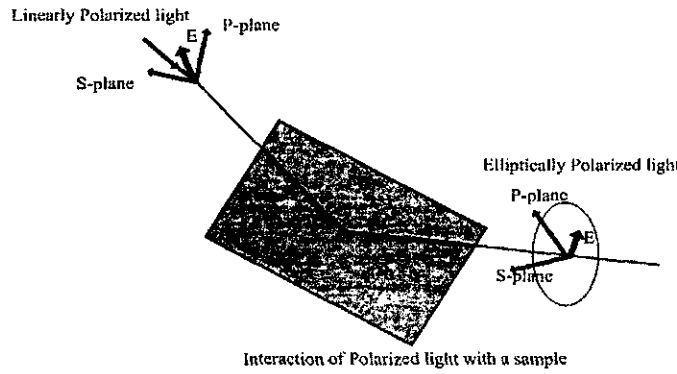

Figure 6.1. Interaction of polarized light with the sample when a linearly polarized light incident on substance.

Variable Angle Spectroscopic Ellipsometry (VASE) in the visible spectral range (420 – 763nm) is carried out using a rotating analyzer, type M-44 (J.A.Woollam Co., Inc., Lincoln, NE, USA) wavelength ellipsometer. Data is fed to a computer and the complex reflection coefficients are analyzed by a regression analysis program, WVASE32. A physical model is created specifying the angle of light incidence, thickness and optical constants of various layers. WVASE32 then calculates the mean squared error (MSE), which is essentially the sum of the squares of the differences between the measured and calculated data for each (Δ,Ψ) pair. A regression algorithm is then used to minimize the MSE by adjusting the values of one or more nominated parameters. The experimental data window is used to load, save and select experimental data for fitting. Most commonly the data will have been acquired using the WVASE32 program. At the time of acquisition, the ellipsometer hardware is unable to distinguish among these multiple ellipsometric data types and by default will store the data as standard ellipsometric data type "E". Reflection mode ellipsometry taken from the top side of the sample. No substrate backside effects will be included in the model calculations. If a layer with anisotropic optical constants is present, the optical axis for that layer will be assumed to be perpendicular to the surface of the sample.

6.1 Data Analysis

Spectroscopic ellipsometry data analysis consists, for the most part, of fitting experimental data to a model, where certain parameters are allowed to float to obtain the best fit. Clearly, this process is critical to getting useful results from spectroscopic ellipsometry experiments. The fitting process consists of three parts:

1. *Select the model* [52]: The number of layers is fixed and basic structure concerning the contents of each layer is set. One must decide if any layer is anisotropic at this stage, and whether or not interface layers are to be modeled as a single effective medium approximation, or is a more complicated graded interface to be used.

2. *Assign optical functions to each layer.* A decision must be made to use existing data sets. The initial values for all parameters and film thicknesses must be assigned, and the floating parameters are selected.
3. *Fit the data.* Model parameters such as thickness (t) are varied in order to fit the experimental data. The root mean squared error (MSE) is used to quantify how well the model fits experimental data. Smaller MSE [53] implies a better model fit thus layer thickness and optical constants are determined where MSE reaches its minimum value. Appropriate film selection is important in getting better fit. Hence fitting with experimental data is started where thin films are transparent (k~0). Then VASE data can be fit with the Cauchy dispersion formula:

$$n(\lambda) = A + \frac{B}{\lambda^2} + \frac{C}{\lambda^4} \tag{6.1}$$

Where A, B, C are fit coefficients and λ is wavelength in nanometers. $k(\lambda) = 0$ in this spectral range. Cauchy dispersion formulae works fine for non absorbing materials. But organic materials are absorbing in visible region hence to get better fit Cauchy fit is used as starting value for Lorentz fit. An accurate determination of optical constants and film thickness of organic materials can be achieved by modeling Lorentz oscillator form as given below

$$\tilde{\varepsilon}(h\upsilon) = \varepsilon_1 + i\varepsilon_2 = \varepsilon_{1_\infty} + \sum_k \frac{A_k}{E_k^2 - (h\upsilon)^2 - iB_k h\upsilon} \tag{6.2}$$

Where hν is the photon energy in eV, $\varepsilon_{1\infty}$ is an additional offset term. A_k is the amplitude, E_k is the center energy, B_k broadening of each oscillator.

Ellipsometry does not directly measure film thickness or optical constants, it measures Psi and Delta. To extract useful information about a sample it is necessary to perform a model dependent analysis of the ellipsometric Psi and Delta data [45].

1. Measurement of ellipsometric angles ψ_{meas} and Δ_{meas}.
2. Data acquired covering the desired spectral range and angles of incidence. A model for the optical structures of the sample is then constructed ψ_{model} and Δ_{model}.

3. Fresnel equations along with the assumed model are used to predict the expected Psi and Delta for the wavelengths and angles of incidence chosen.
4. The fourth part of the process described is to compare the actual measured Psi and Delta with the predictions of the model based on Fresnel equations assuming values of the optical constants and thicknesses.

Model used to measure optical parameters as well as data analysis after modeling is shown in figure below. We use Biaxial.mat to measure properties of optical layer. Here two cauchy layers are used to create effective anisotropic model.

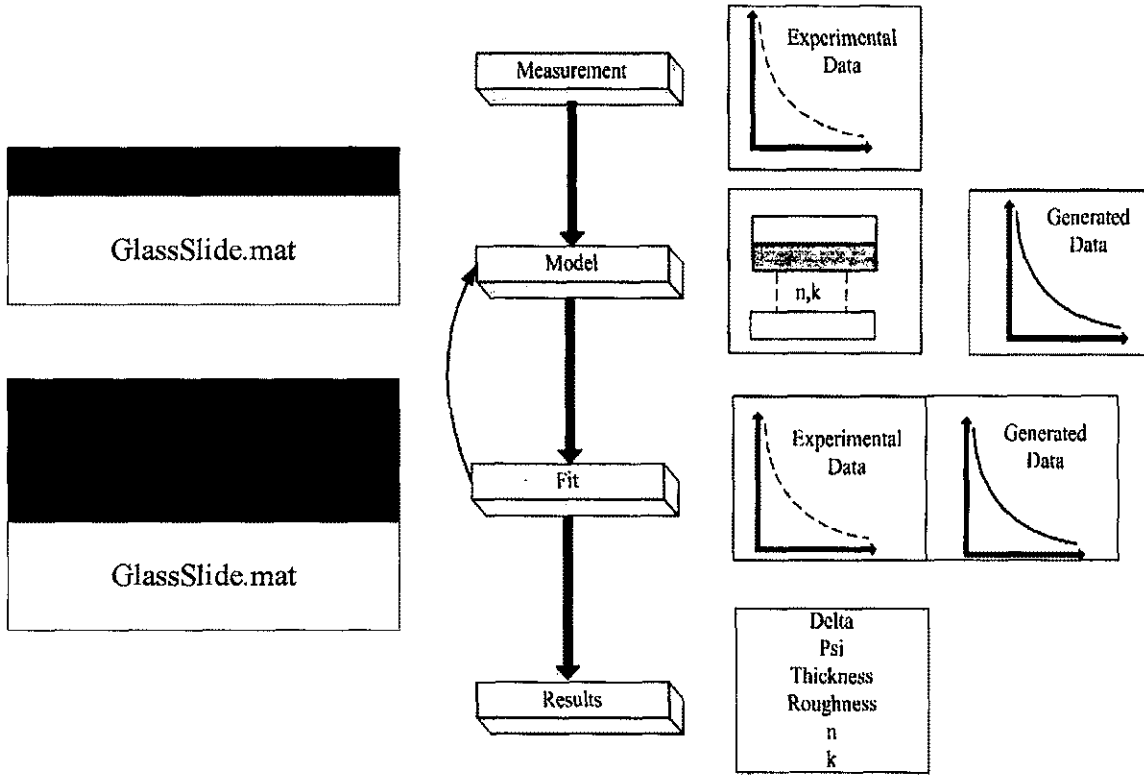

Figure 6.2. Ellipsometry Data Analyses [41].

6.2 Dielectric Function (ε)

From Maxwell's equation, $$\Delta E = \frac{\mu\varepsilon}{c^2}\frac{\partial^2 E}{\partial t^2} \tag{6.3}$$

Where c, μ, ε are velocity of light, magnetic permeability and dielectric function (DF) respectively. $n = \sqrt{\mu\varepsilon}$ (6.4)

For most of semiconducting and insulating materials magnetic permeability μ is nearly unity [41]. Then the refractive $n = \sqrt{\varepsilon}$. In order to describe absorbing materials, a complex dielectric function $\acute{\varepsilon} = \varepsilon_1 + i\,\varepsilon_2$ and complex refractive index $\acute{n} = \sqrt{\acute{\varepsilon}} = n + ik$ are introduced. The imaginary part of DF cannot be taken as zero. The intensity of the wave decays as it propagates

$$I \sim E^2 \sim \exp\left(-\frac{4\pi k z}{\lambda}\right) \quad (6.5)$$

Comparing equation 6.3 with Beer-Lambert's law $I(z) = I(0)\exp(-\alpha z)$ (6.6)

We find that the absorption coefficient $\alpha = \frac{4\pi k}{\lambda}$ (6.7)

substituting equation 6.2 $\varepsilon_2 = 2nk$ and $\lambda = 2\pi c/\omega$ in 6.5 we obtain

$$\alpha = \frac{\varepsilon_2 \omega}{nc} \quad (6.8)$$

The complex dielectric function is one representation of the optical constants of a material. It is defined as the ratio of the displacement field to the applied electric field at a given point in a material and is a measure of how polarizable a material is at the given wavelength (or photon energy). The imaginary part of the dielectric function is a measure of how much energy per unit volume and unit time a material will absorb from a light beam of the given wavelength.

Continuous exposure of UV radiation degrade polymer device performance and in UV region (<320nm) dielectric function of films is nearly isotropic hence spectroscopic ellipsometry experiments are done in visible region only. In the visible region (<320nm) however, the changes of the dielectric function are much stronger. The figures shows experimental SE spectra of the pseudodielectric function for P3HT and P3HT:PCBM composite films. As acquired, SE spectra doesnot fit exactly with experimental data due to presence of interference fringes caused by multiple reflections at the substrate/film

interface. From ellipsometry experiments we observed that for P3HT, P3HT:PCBM films dielectric function is shifted towards lower photon energies (higher wavelengths – red shift) and dielectric function ε_2 enhanced upon annealing at 150^0C. Polymer films made from P3HT:PCBM-C_{70} shows much improved absorption spectrum as well as improved dielectric function compared to P3HT:PCBM-C_{60}.

6.2.1 P3HT Dielectric Function (ε)

Figure 6.3 shows the real and imaginary dielectric function of P3HT before and after annealing versus wavelength. From equation 6.6 it is clear that the imaginary dielectric function and absorption are directly proportional. As the annealing temperature increases the degree of inter chain and intra chain ordering in films of P3HT increases which leads to enhanced absorption band with more pronounced vibrational structures. With annealing, films become denser which also leads to increase in dielectric function.

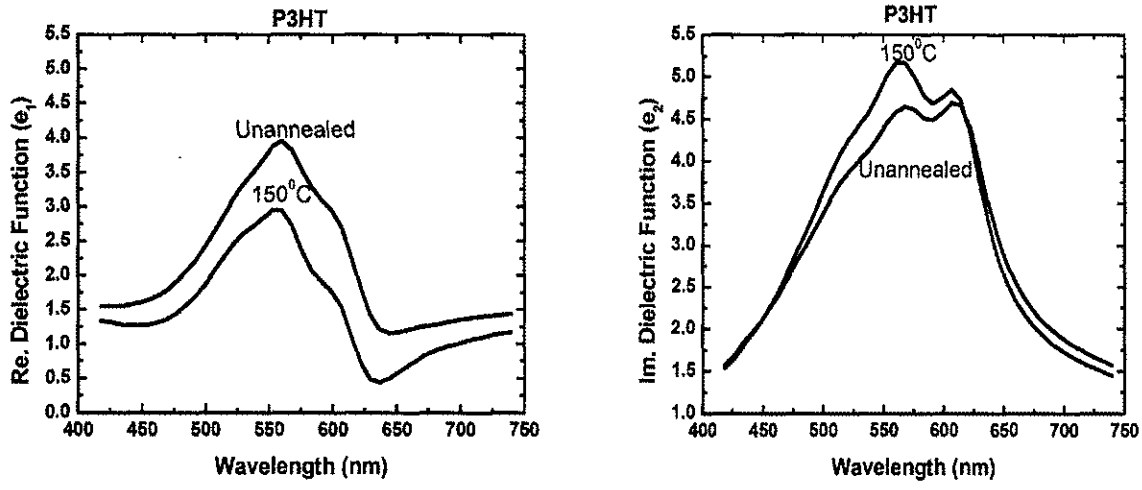

Figure 6.3. Real and Imaginary dielectric functions vs., wavelength of P3HT before and after annealing at elevated temperatures for same film thickness.

6.2.2 P3HT:PCBM Dielectric Function (ε)

The dielectric Function of P3HT:PCBM composites upon annealing show intrinsic peaks owing to P3HT in certain range. Figure 6.4 shows dielectric function ε_2 of P3HT:PCBM-C_{60}. DF decreased in intensity, but peaks and shoulders are enhanced when compared to

P3HT films. The spectrum goes high below 400nm where PCBM shows its highest absorption (~320nm). From absorption measurements PCBM has absorption peak at 320nm.

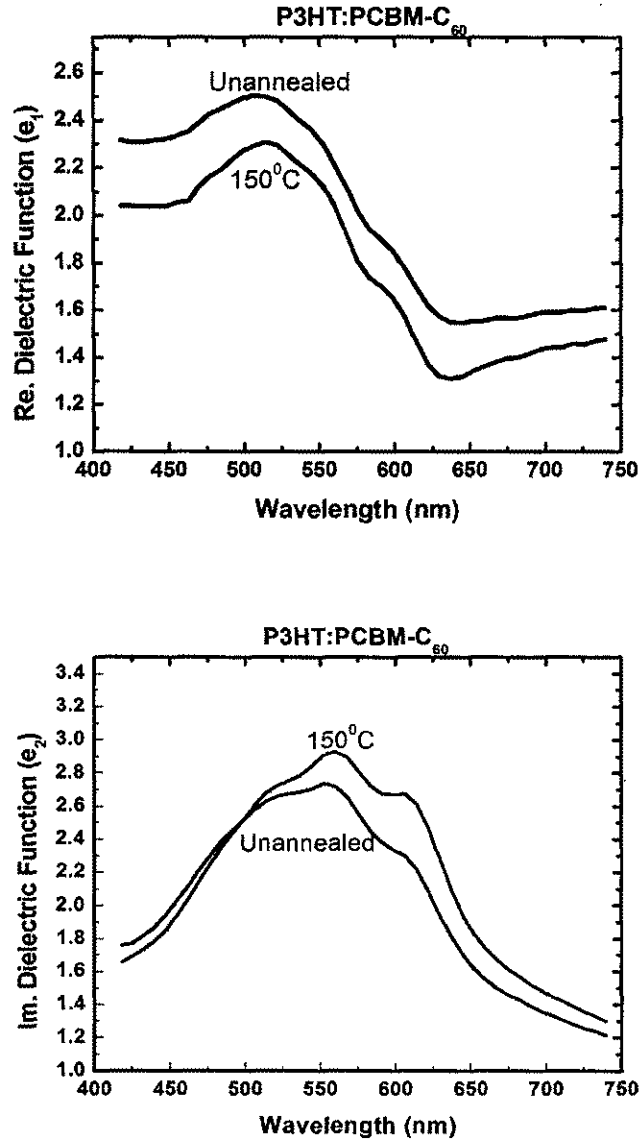

Figure 6.4. Real and Imaginary dielectric functions vs., wavelength of P3HT:PCBM-C_{60} before and after annealing at 150^{0}C inside nitrogen glove box. Peaks are enhanced in comparison with P3HT.

Dielectric function ε_2 of P3HT:PCBM-C_{70} shown in figure 6.5. DF of P3HT:PCBM-C_{70} enhanced when compared to its analogous P3HT:PCBM-C_{60}. The reason attributed to this

phenomenon is the asymmetry in PCBM-C_{70} it can easily transfer charge when mixed with P3HT which enhances absorption as well as device performance.

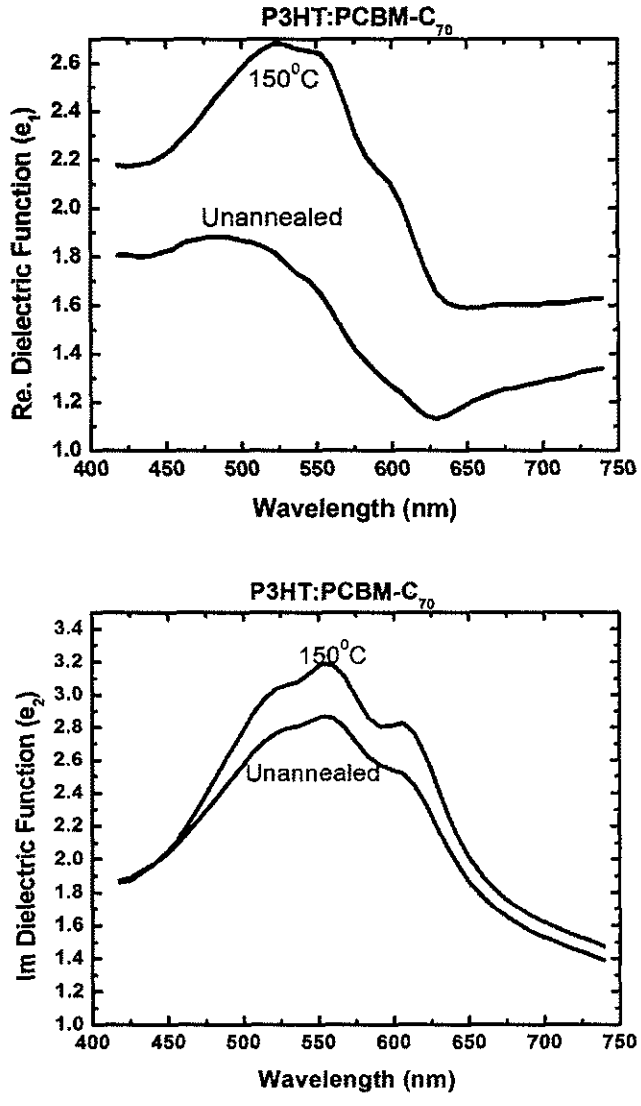

Figure 6.5. Real and Imaginary dielectric functions vs., wavelength of P3HT:PCBM-C_{70} before and after annealing at 150^{0}C inside nitrogen glove box.

The Real and Imaginary part of dielectric function for P3HT and P3HT:PCBM composites are compared to see the variation. Figure 6.5 shows ε_2 as function of photon energy for thin films at same standard conditions.

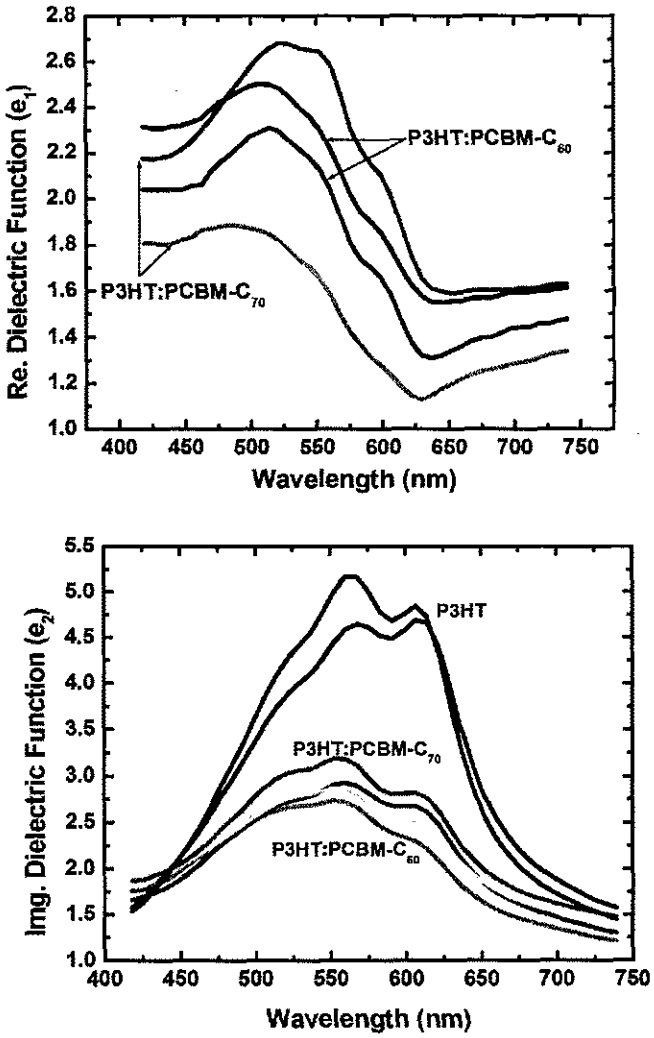

Figure 6.6. Real and Imaginary dielectric functions vs., wavelength of P3HT, P3HT:PCBM (C_{60}, C_{70}) composites before and after annealing at 150^0C inside nitrogen glove box. Enhanced dielectric function observed in P3HT:PCBM-C_{70} compared to its analogous P3HT:PCBM-C_{60}.

6.4 Complex Index of Refraction (ń)

In real materials the polarization does not respond instantaneously to an applied field. This causes dielectric loss, which can be expressed by a permittivity that is both complex and frequency dependent. Real materials are not perfect insulators either; they

have non zero direct current conductivity. Taking both aspects into consideration we can define a complex index of refraction as ń=n+ik. It governs the phase change and amplitude decay of a plane electromagnetic wave propagating in the material. **n** is the refractive index indicating how fast the phase of the propagating wave changes while **k** is the extinction coefficient that determines how fast the amplitude of the wave decreases as the wave propagates (absorption loss when the electromagnetic wave propagates through the material). Both n, k is dependent on wavelength. The complex index of refraction is one representation of the optical constants of a material.

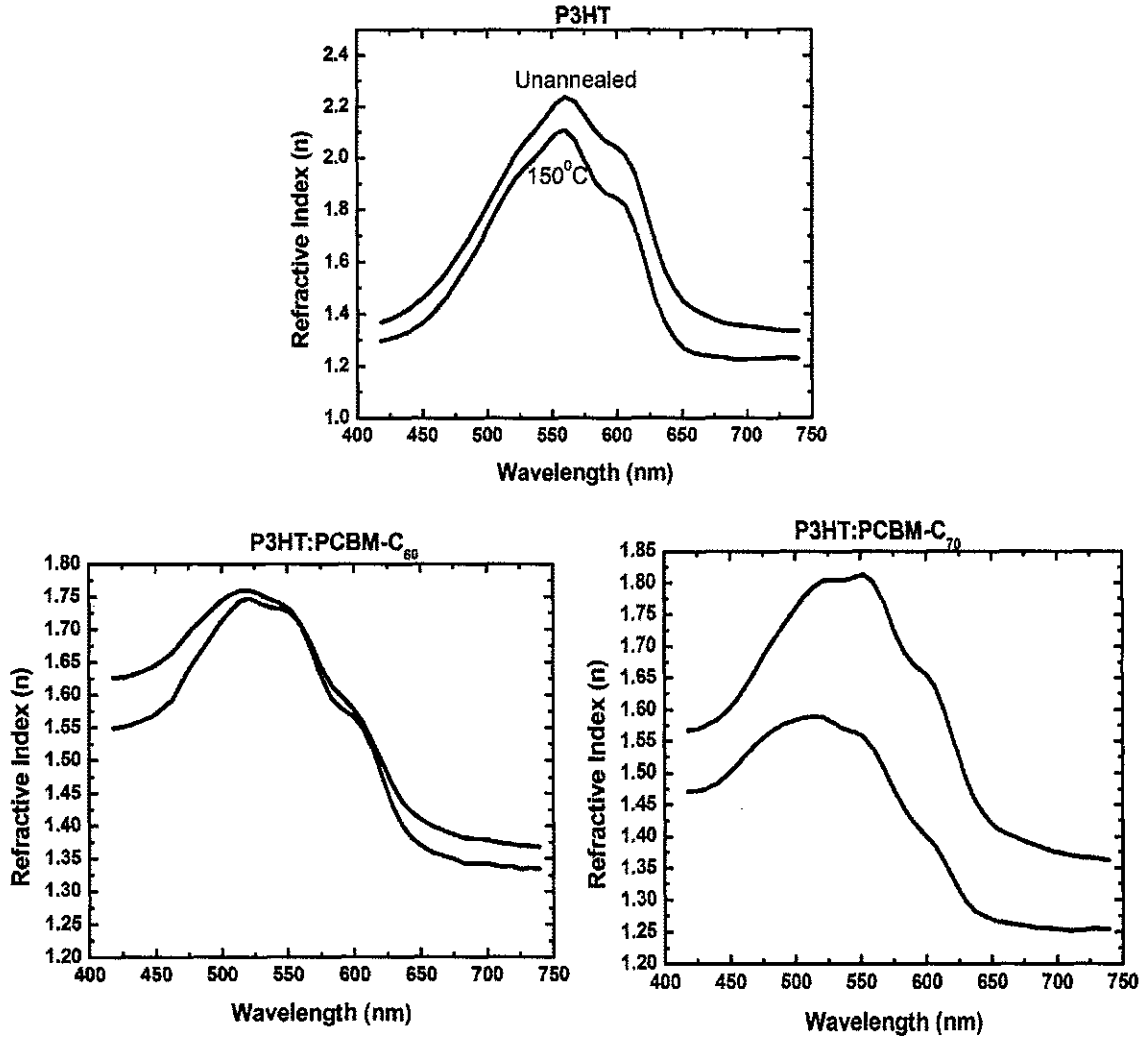

Figure 6.7. Refractive Index vs., wavelength of P3HT and P3HT:PCBM composites before and after annealing at elevated temperatures for same film thickness.

The Extinction coefficient k is the imaginary part of the complex index of refraction and governs the rate at which a propagating wave will decay as it propagates. If k is zero the amplitude of the wave will remain constant as the wave propagates and the material is said to be transparent.

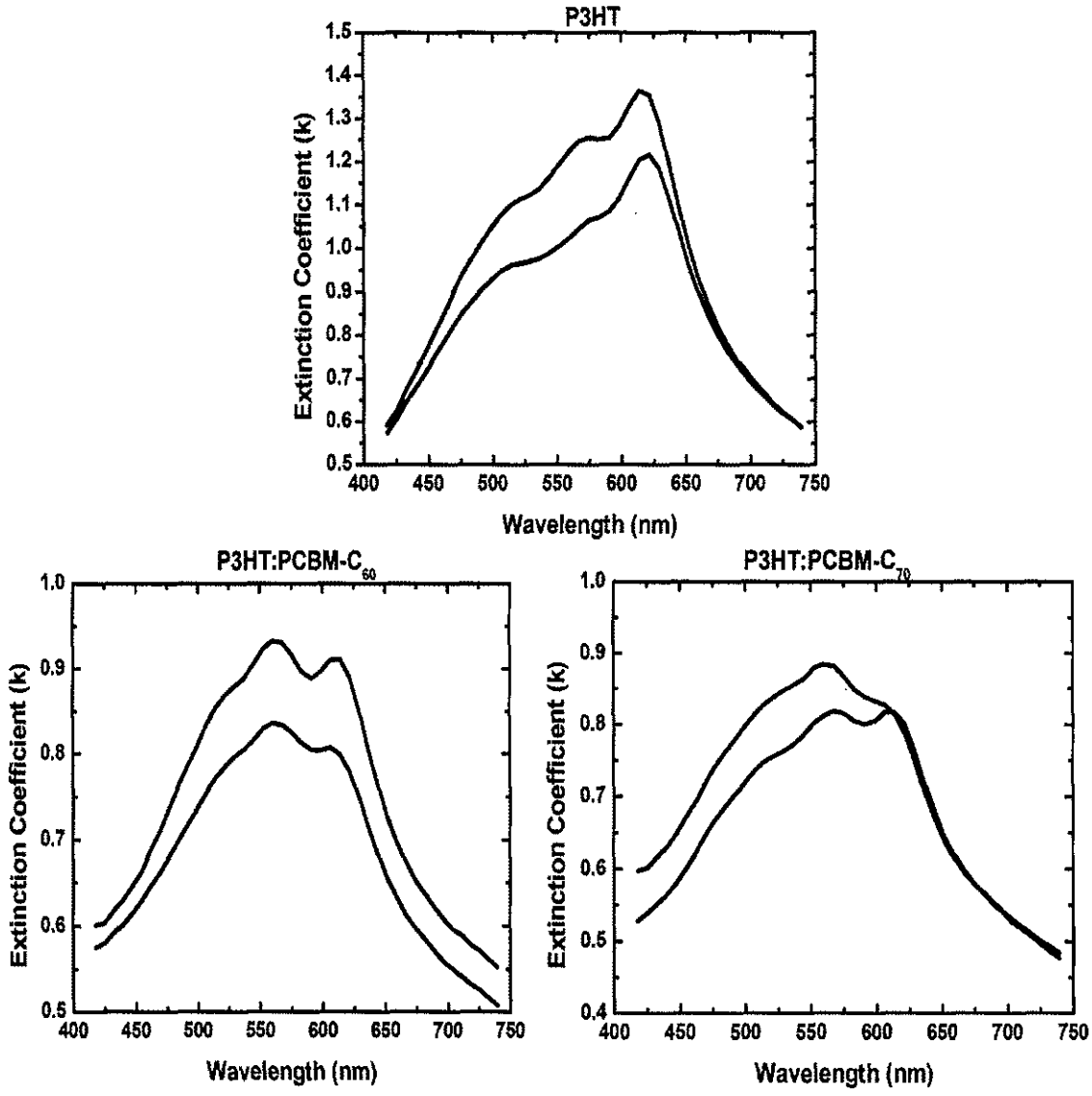

Figure 6.8. Refractive Index vs., wavelength of P3HT and P3HT:PCBM composites before and after annealing at elevated temperatures for same film thickness.

CHAPTER VII

ATOMIC FORCE MICROSCOPE

An Atomic Force Microscope (AFM) or scanning force microscope (SFM) is a very high resolution type of scanning probe microscope, with demonstrated resolution of fractions of a nanometer. In the case of the STM a tunneling current is controlled between a relatively sharp tip and the sample and thus conducting samples and/or substrates are required. However AFM requires no conductivity; tip sample interactions are based on mechanic short or long range forces. Basic AFM modes of operation are [54]

1. *Contact Mode*

   Tip is scanned across the surface to measure the deflection and adjusts accordingly.

2. *Non Contact Mode*

   Oscillating cantilever scheme is employed. Detection is based on measuring resonant frequency or amplitude of the cantilever.

3. *Dynamic Force / Intermittent-contact / Tapping mode*

   Cantilever is oscillated closer to the sample. Tip intermittently touches or taps the surface.

   Both non-contact mode and tapping mode use extended tip sample interactions via Vander Waals long-range forces [55] [56].

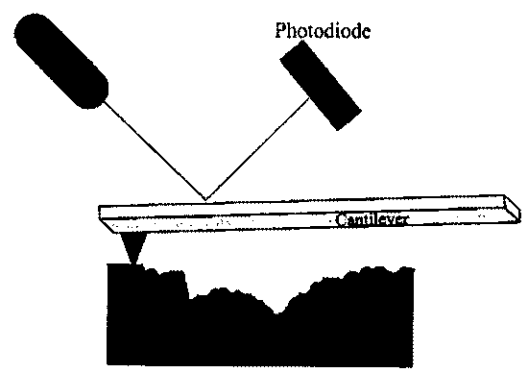

Figure 7.1. Basic principle of Atomic Force Microscope showing cantilever oscillations and amplitude detection of cantilever using split photodiode and detector.

Tapping mode offers less destructive measurements at a higher resolution for soft organic materials. Quartz piezo is used to excite the cantilever to oscillate. Feedback is used to maintain constant distance from the surface. The feedback loop maintains constant amplitude of the cantilever oscillation and this amplitude is detected via a reflected laser spot unto a split photodiode detector [55]. One of the advantages of AFM is its ability to magnify in the X, Y, Z axes. Figure 7.2 shows several types of microscope and profilometers

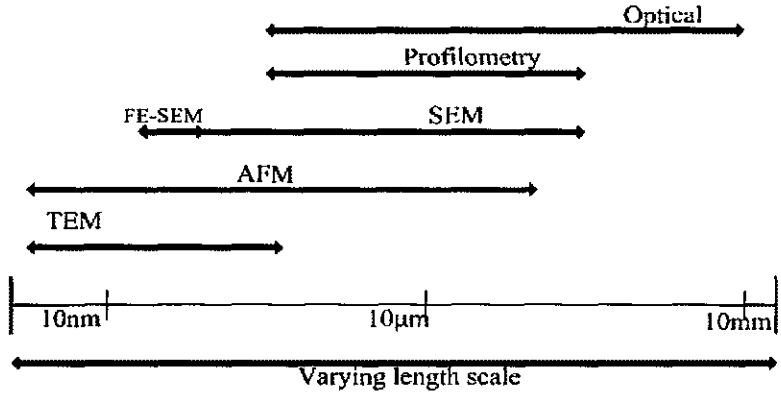

Figure 7.2. Imaging scale comparison of different 2-D, 3-D profiling and imaging instruments. AFM enables to resolve features from few nm ranges to mm range.

AFM is typically combined with optical microscope to select location during scanning. AFM is compared with electron beam techniques such as TEM, SEM. It is simple to prepare samples and no need of vacuum which makes this technique suitable for organic materials. An atomic force microscope (AFM) creates a highly magnified three dimensional image of a surface. The magnified image is generated by monitoring the motion of an atomically sharp probe as it is scanned across the surface. With AFM it is possible to see features on a surface having few nanometer range and single molecules on the surface. Figure 7.3 shows major components of AFM 1. Microscope stage 2. Computer monitors 3. Electronic controller

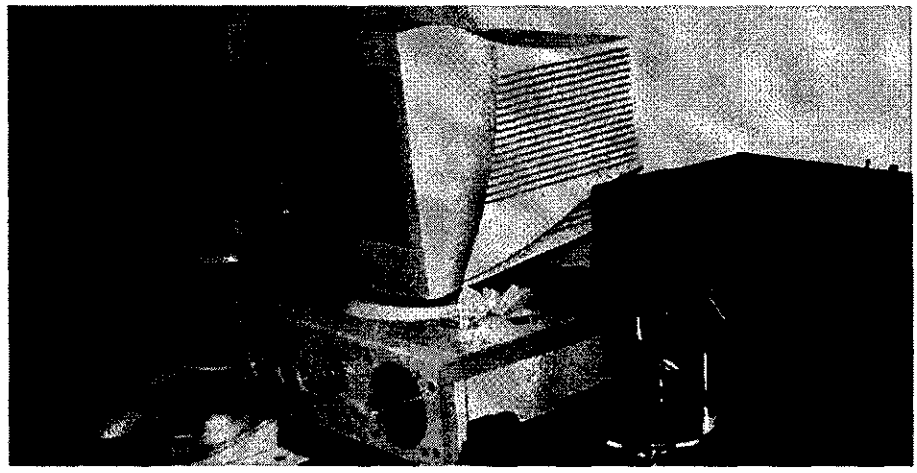

Figure 7.3. Laboratory setup of the Dimension 3100 SPM in tapping mode including scanner, sample display, screen, control screen, processor and image display.

AFM experiments were performed with a Digital Instruments Multimode/ Nanoscope III scanning probe microscope. The surface images were obtained simultaneously while operating the instrument in the tapping mode under ambient conditions. Images were taken at the fundamental resonance frequency of the Si cantilevers (300 kHz). Typical scan speeds during recording were 0.3 - 0.5 KHz.

7.1 Thermal Annealing

Berggren et al. showed that thermal annealing can enhance the polymer crystallinity [57]. Regio Regular P3HT crystallization starts to appear at annealing temperatures as low as 40^0C [58]. Mild thermal treatment enhances external quantum efficiency when compared to untreated device. An important issue in these devices is the phase structure formed by the mixture of the different components; the efficiency is ruled by the active layer film morphology [63-67].

7.2 Morphology

The BHJ structure of organic photovoltaics consists of 3D interpenetrating networks of donor and acceptor materials. AFM images of the polymer film surface

before and after annealing at different temperatures are shown in figure 7.4. The surface of as cast pristine P3HT film is very smooth with RMS roughness 0.414nm.

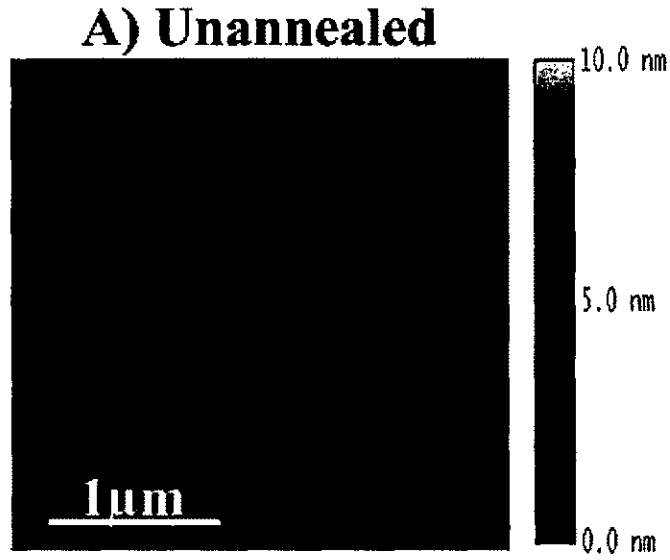

Figure 7.4. (Color Online) Surface morphology of pristine P3HT thin film (~200nm) as cast from chlorobenzene solution (1:1wt %).

After undergoing thermal treatment the roughness first increases to 110^0C and then decreases [59-62]. The highest roughness is obtained at 150^0C. Film texture also changes up on annealing of as cast films. The film annealed above 100^0C forms broad hill like features compared to films annealed below 100^0C. Higher film roughness gives higher device efficiency. Therefore, the increased surface roughness play direct role in efficiency improvement. Higher surface roughness is more likely a signature of annealing enhanced ordered structure formation in the polymer film. Up on annealing of films absorption as well as charge carrier mobility increases which in turn enhance device performance. Figure 7.5 shows the surface morphology of annealed pristine P3HT thin films. Lighter areas correspond to the harder, crystalline material.

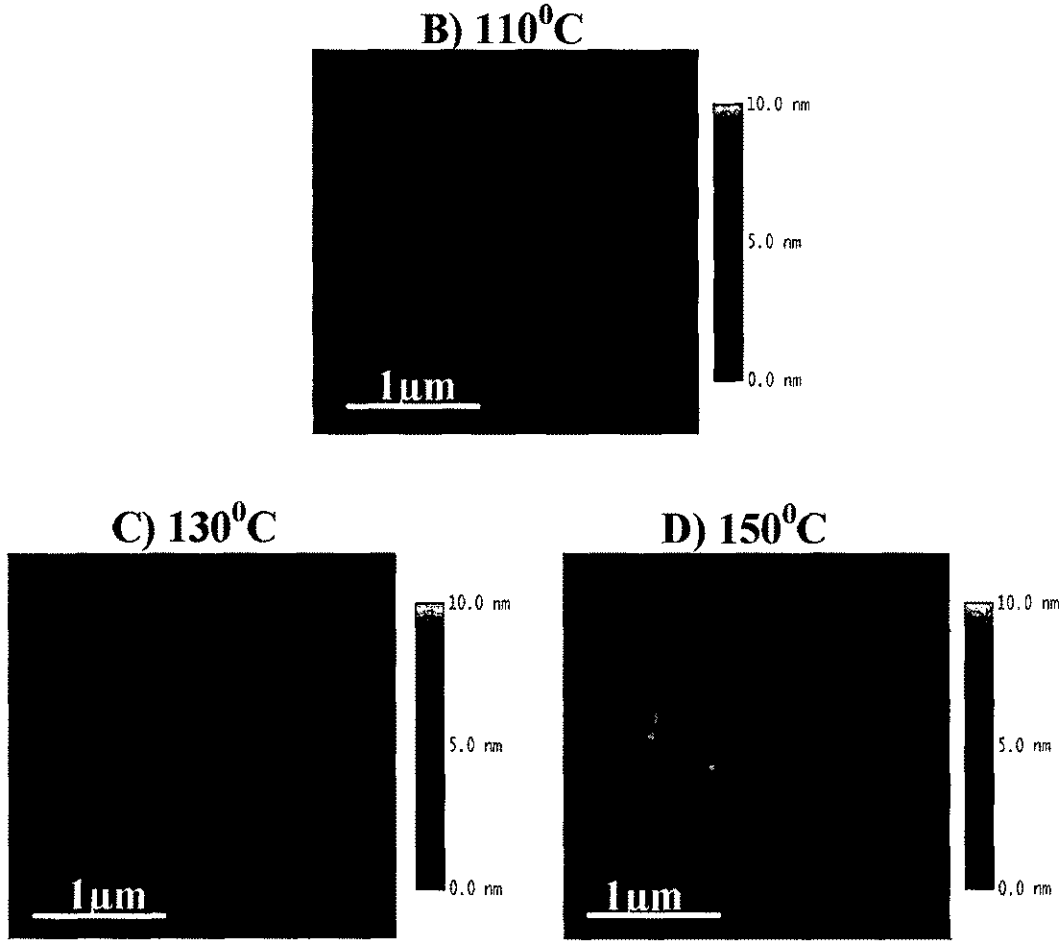

Figure 7.5. (Color online) AFM images showing surface morphology of pristine P3HT thin film (~200nm thick) spin coated on glass slide. Films are spun from chlorobenzene solution (1:1wt%). Annealed at temperatures B)110^{0}C, C)130^{0}C, D)150^{0}C for 10min inside N_2 glove box with O_2 & H_2O ppm levels below 0.1ppm.

Films produced by spin coating display a non-equilibrium structure with reduced order and orientation. Annealing of P3HT films leads to semi crystalline structures and forms needle like crystallites. The figure below shows annealing P3HT films at temperatures above 100^{0}C. Films become crystalline as annealing temperatures increase. Surface morphology studies show that in thin films of pristine P3HT self assembly is controlled by a complex interplay of microphase separation, surface induced orientation, crystallization and molecular mobility. We understand the preferred orientation of the

crystallites parallel to the substrate as a result of interfacial interactions, which leads to an alignment of the liquid crystalline phase parallel to the substrate. Initially, the spin coated films are far from equilibrium due to the rapid formation of the film. At higher temperatures, the mobility of the polymer chains increases, allowing the crystals to grow and to orient in a specific direction which enhances device performance. Cast and annealed PCBM-C_{60} films are shown in figure 7.5. As the temperature increases PCBM-C_{60} forms into bigger crystallites.

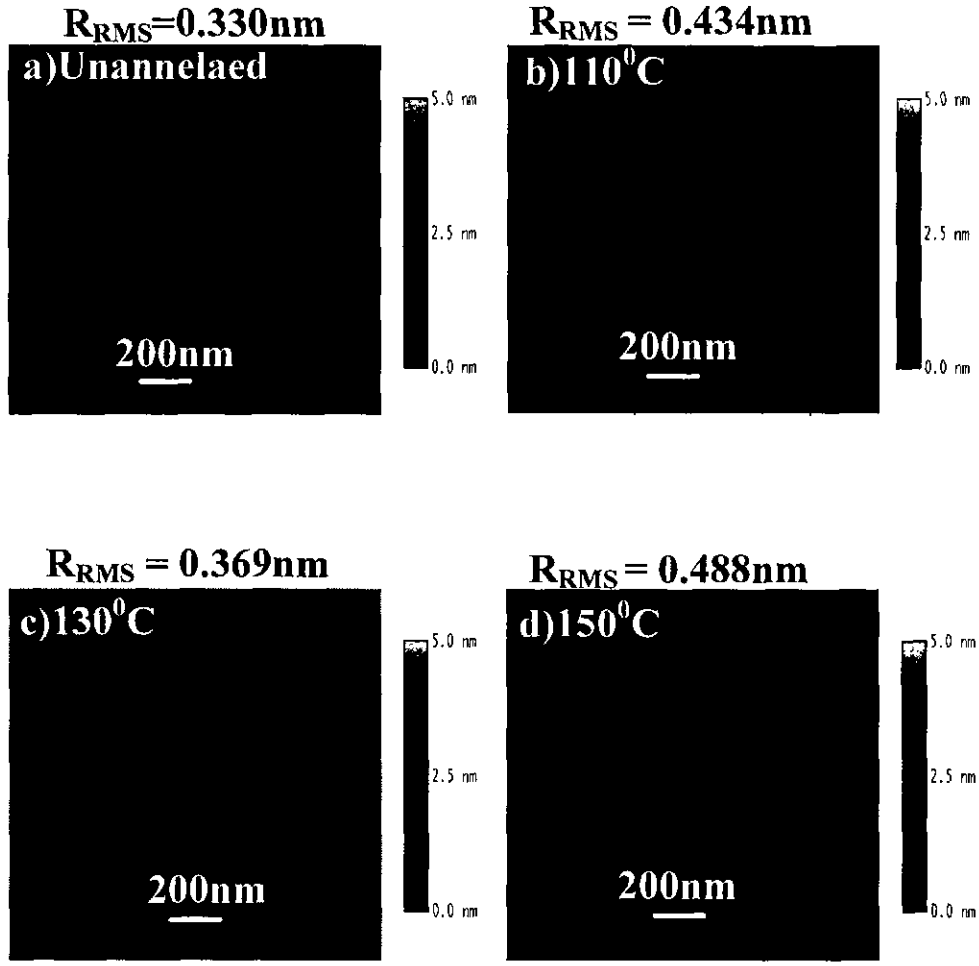

Figure 7.6. (Color online) AFM surface images of PCBM-C_{60} thin film spin coated on glass slide. Unannealed and annealed at temperatures b)110^{0}C, c)130^{0}C, d)150^{0}C for 10min inside N_2 glove box.

Instead of forming bigger crystallites like PCBM-C_{60}, PCBM-C_{70} shows a small increase in surface roughness. The surface morphology appears to be forming crystallites with small nanodomains.

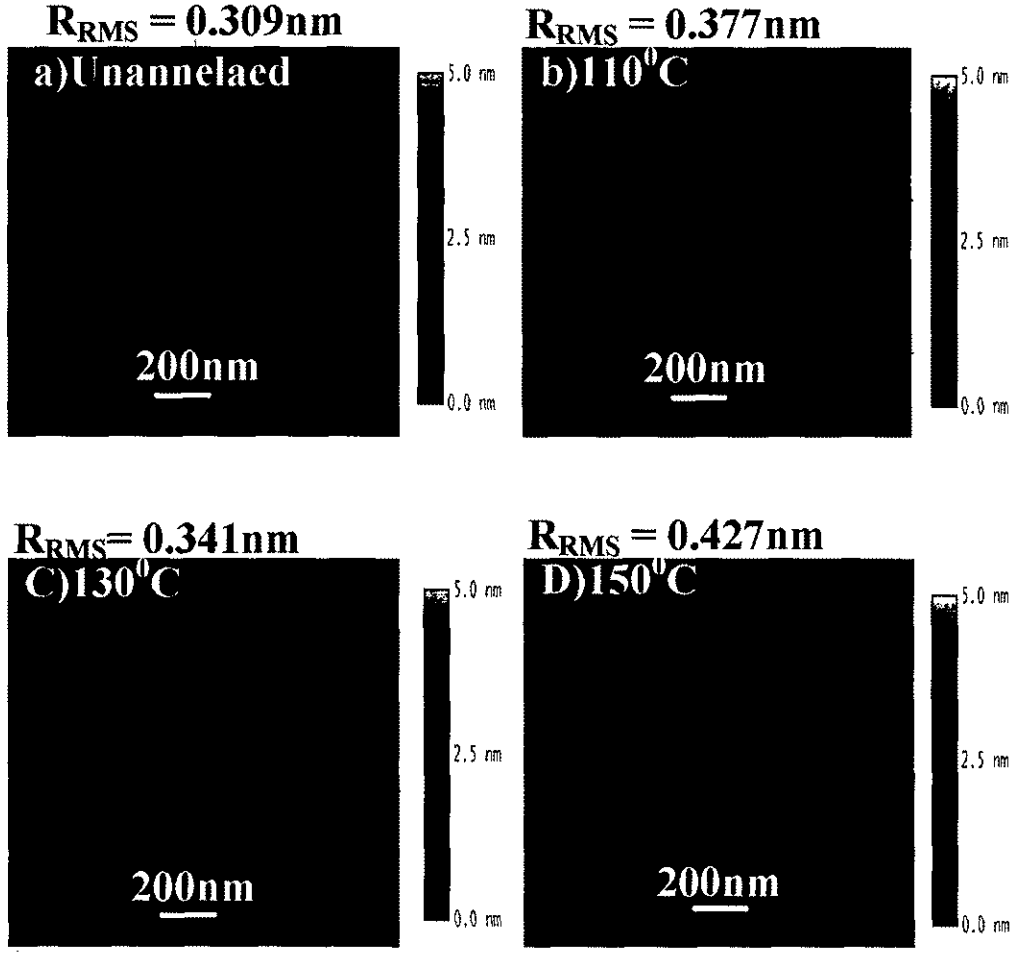

Figure 7.6 (Color online) AFM surface images of PCBM-C_{70} thin films as cast from chlorobenzene solution (1:1 wt%). Unannealed and annealed at temperatures b)110^{0}C, c)130^{0}C, d)150^{0}C for 10min inside N_2 glove box.

Charge transport in polythiophene: fullerene composites are typically a hopping process that is thermally activated. The thermal annealing proceess significantly improves the efficiency [15,16] of RR-P3HT:PCBM solar cells by improving the morphology. Upon annealing

1. The density of organic film increased
2. Enhancement in intermolecular interaction which leads to improved absorption
3. Better electrical charge transport by increasing charge carrier density
4. Optimized phase segregation by enhancing the diffusion of methanofullerene molecules in the polymer matrix when heated above glass transition temperatures.
5. Solvent concentration removal by evaporation which in turn leads to less defect areas.

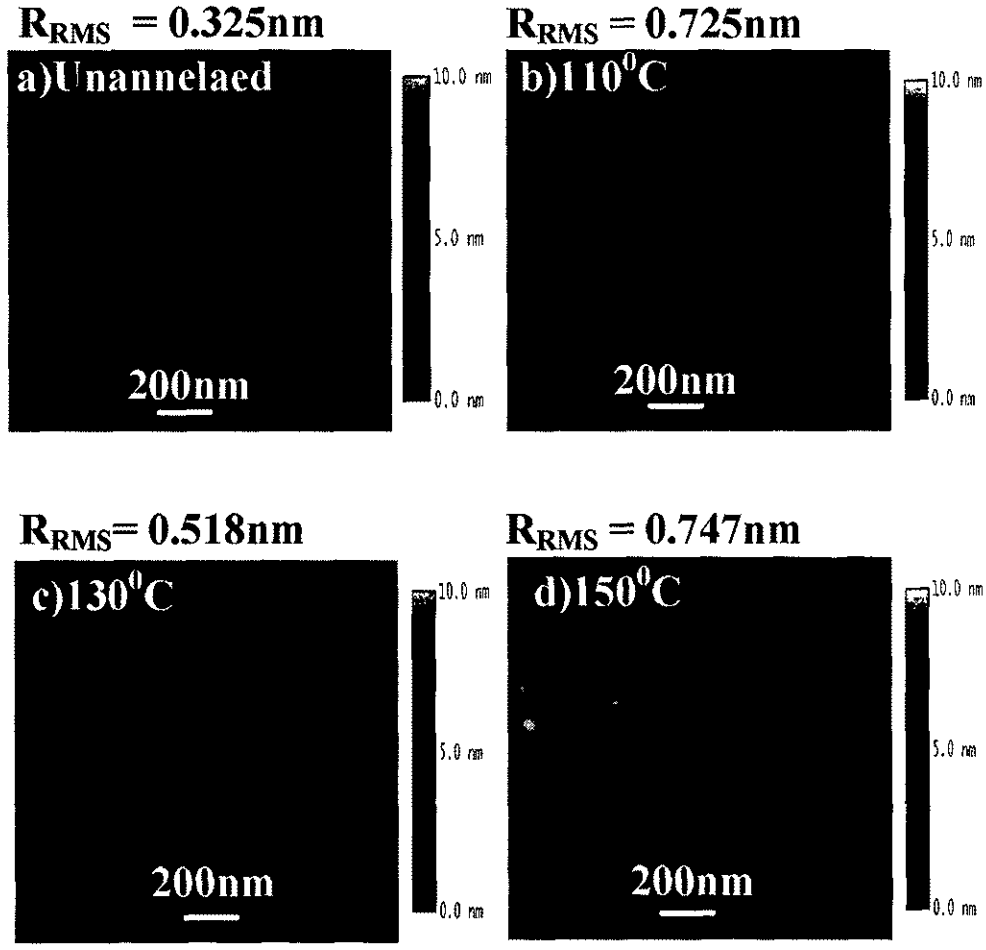

Figure 7.8. (Color online) AFM surface images of P3HT:PCBM-C_{60} (1:1) thin film as cast from chlorobenzene solution (1:1wt%). Unannealed and Annealed at temperatures b)110^{0}C, c)130^{0}C, d)150^{0}C for 10min inside N_2 glove box with O_2 & H_2O ppm levels below 0.1.

Surface roughness for each annealed sample is measured. RMS surface roughness is plotted against annealing temperature. The highest roughness yields better contact with metal electrodes, better charge transport, improved absorption and improvement in conductivity of films. Figure 7.9 shows RMS roughness versus annealing temperature where films are annealed inside nitrogen glove box with H_20, O_2 ppm levels below 0.1. There is significant decrease in roughness when samples are annealed at 130^0C. The reason may be attributed to evaporation of chlorobenzene solvent at 132^0C, which makes the film smooth and less rough. Almost the same roughness observed at annealing temperatures 110^0C and 150^0C.

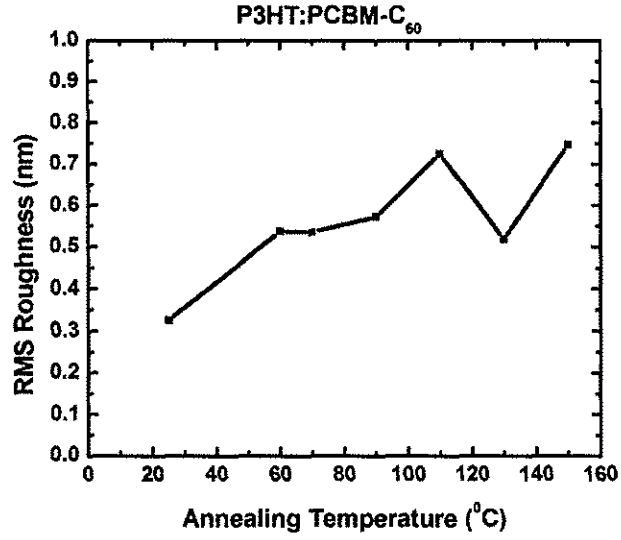

Figure 7.9. RMS roughness vs. annealing temperatures. All samples are annealed inside nitrogen glove box to prevent interaction with ambient atmosphere.

Surface morphology and RMS roughness versus annealing temperature for P3HT:PCBM-C_{70} films are shown below. Variation in surface roughness is much less when compared to P3HT:PCBM-C_{60}.

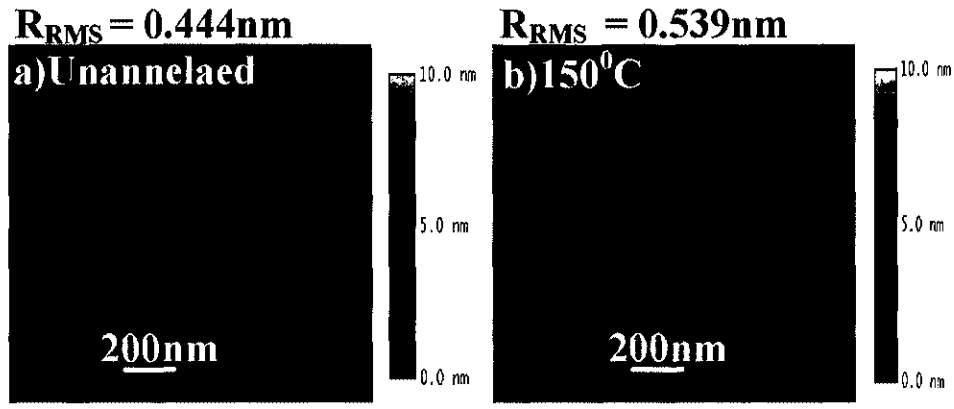

Figure 7.10. (Color online) AFM surface images of P3HT:[70] PCBM (1:1) thin film spin coated on glass slide. Films are spin cast from chlorobenzene solution 10mg/ml. Unannealed and annealed at temperatures b)60^{0}C, c)70^{0}C, d)90^{0}C, e)110^{0}C, f)130^{0}C, g)150^{0}C for 10min inside N_2 glove box.

Annealing temperatures versus surface roughness of P3HT:PCBM-C_{70} are shown in figure 7.11. Roughness of P3HT:PCBM-C_{70} films are less compared to P3HT:PCBM-C_{60}. There isnot much variation in roughness before and after annealing.

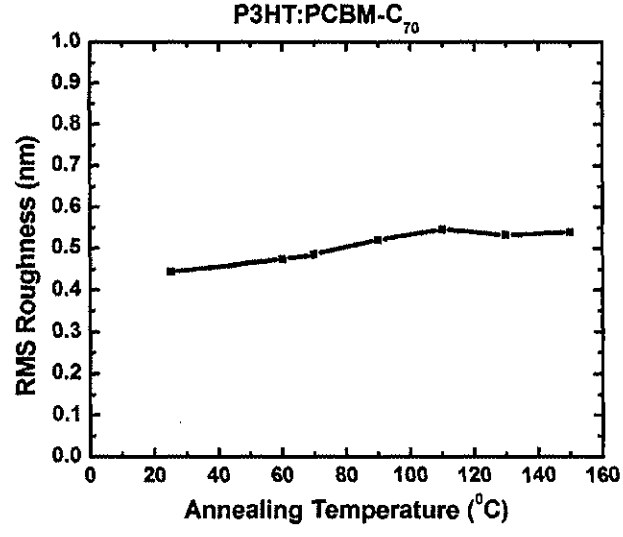

Figure 7.11. RMS roughness vs. annealing temperatures for P3HT:PCBM-C_{70}.

CHAPTER VIII

CORRELATION BETWEEN UV-Vis, SE and AFM DATA

8.1 Effect of annealing on surface morphology

Figure 8.1 shows tapping mode AFM results obtained on untreated and annealed pristine P3HT, PCBM (C_{60} & C_{70}) and P3HT: PCBM (C_{60} & C_{70}) composites. A moderate surface roughness is observed for non annealed films. In the case of annealed samples the surface gets somewhat rougher. Table 8.1 shows surface roughness comparison for non-annealed and annealed samples.

Table 8.1 shows surface roughness comparison for non-annealed and annealed samples.

	Roughness of Non Annealed films	**Roughness of Annealed films**
P3HT	0.312	0.568 (150^0C)
PCBM-C_{60}	0.33	0.488 (150^0C)
PCBM-C_{70}	0.309	0.427 (150^0C)
P3HT: PCBM-C_{60}	0.325	0.747 (150^0C)
P3HT: PCBM-C_{70}	0.414	0.584 (150^0C)

Annealing at elevated temperatures enhances device performance by improving surface morphology. Roughness of thin films is increased and increased crystallization can be observed from tapping mode AFM topographic images. Thus, the annealing of P3HT/PCBM composite films leads to better phase separation in a conjugated polymer: fullerene blend, resulting in the formation of the polymer crystallites. The increased crystallinity in composite polythiophene:fullerene films is supported by diffractogram studies on untreated and annealed films at 150^0C for 10 min.

8.2 Effect of annealing on optical properties

8.2.1 UV-Vis Absorption

The growth of polymer crystallites upon annealing leads to a drastic change of optical properties in P3HT:PCBM composites. In the UV spectral region (~320nm), the absorption coefficient is mainly determined by the optical transition of the PCBM. From UV-Vis studies it shows that there is not much change in peak of PCBM upon annealing, which shows that PCBM is amorphous.

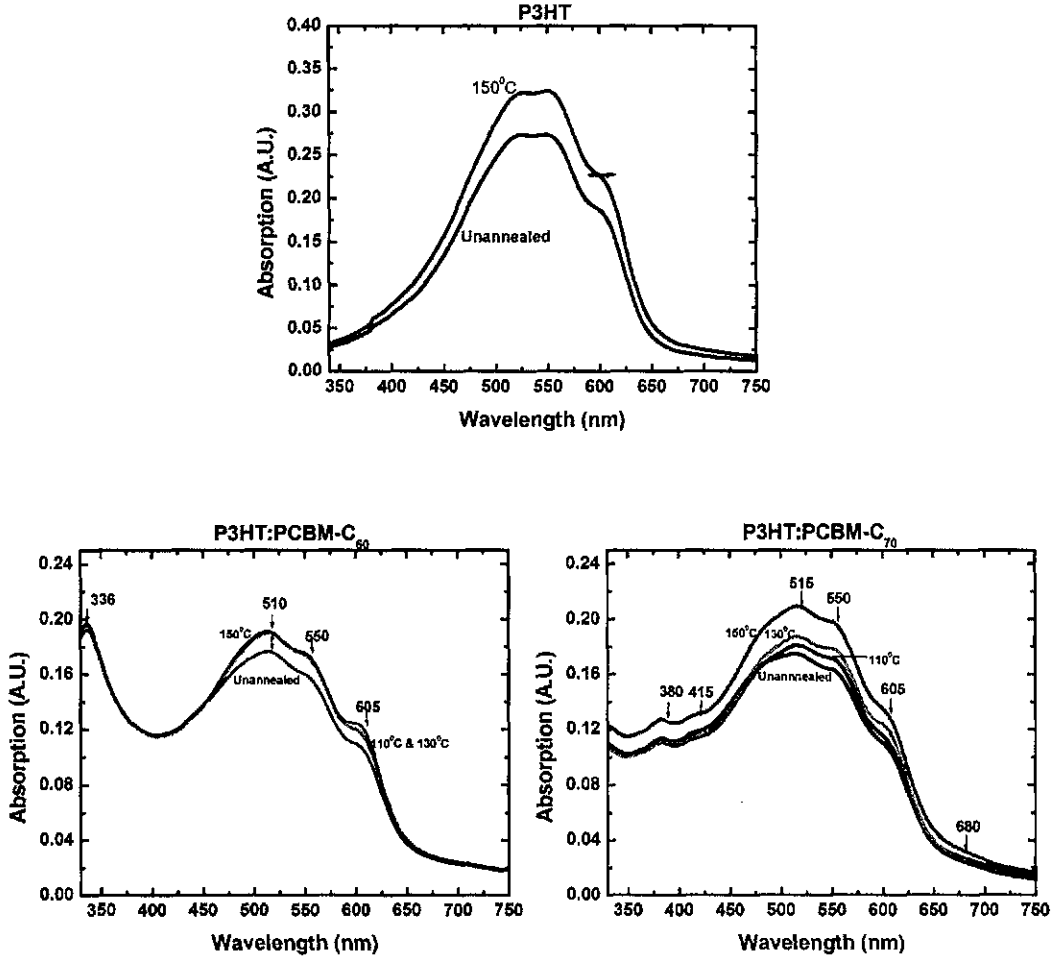

Figure 8.2. UV-Vis absorption spectrum of pristine P3HT, and P3HT:PCBM composites.

The absorption measurements, correlated with the morphology investigations [70-72][75] pointed out that there is a change in the physical conformation of the P3HT chains upon

annealing at elevated temperatures. As a result, the packing of P3HT together in the presence of PCBM relative to pristine P3HT films changes, thereby adapting the relevant optical and electronic properties that are critical for enhancing device performance. Annealing at elevated temperatures enhances absorption of the active layer, which is attributed to formation of crystallized structure in polythiophene: fullerene composites.

8.2.2 VASE

Important differences between the dielectric function of annealed and unannealed films in visible region (<3.2eV) are

1. The imaginary part of the DF ε_2 is shifted towards the lower photon energies around 2.5eV.
2. DF ε_2 increased upon annealing.

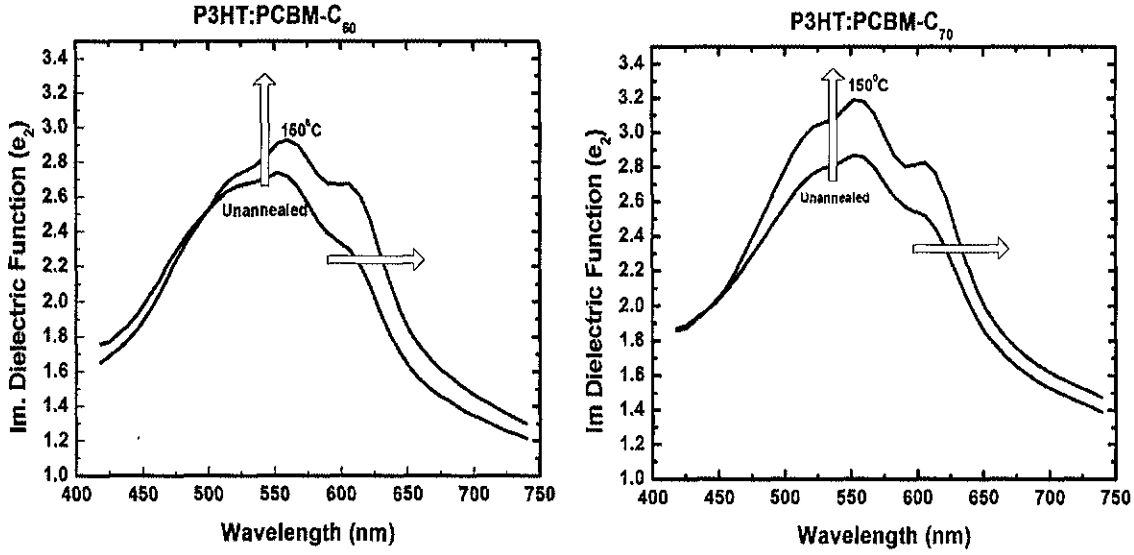

Figure 8.3. Dielectric Function enhancement and shift towards low photon energies for polythiophene:fullerene composites upon annealing.

It has been observed that both absorption and emission maxima of conjugated polymers are shifted towards lower photon energies (longer wavelength) with an increase in conjugation length [73,74]. Due to annealing, polymer: fullerene composites crystallize. The conjugation length in crystallized films is larger because the polymer molecules

within such crystallites are perfectly oriented and there are no defects like chain kinks that limit the conjugation length. Thus, the mean conjugation length for annealed samples should be larger, resulting in the observed shift of the absorption peaks towards lower photon energies (longer wavelengths). We attribute the increase in the optical absorption to the change of the state of the aggregation of the P3HT from amorphous to nanocrystalline upon annealing [76]. Due to crystallization, the interaction between the P3HT molecules becomes stronger.

CHAPTER IX

I-V CHARACTERISTICS MEASUREMENT

9.1 I -V Characteristics

The device performance is determined by IV measurements. Basic setup, measurement methods and their automation are described in this chapter. The current-voltage measurement is the standard measurement for characterizing solar cells. A linear voltage sweep *-1* to 2V is applied to OSC, and the resulting I in the circuit is measured. Current density (J) is the intensive factor in solar cells that vary from device to device. The measurement is carried out both with and without illumination. Without illumination, the device shows a diode behavior. Under illumination, extra charge carriers are generated in the active layer which enhances photocurrent. The J-V curve is shifted down by the amount of the photocurrent (J_{ph}). Key parameters of solar cell can be determined from the J-V curve.

$$\text{Fill Factor FF} \equiv \frac{J_m * V_m}{J_{sc} * V_{oc}} \tag{9.1}$$

The power conversion efficiency η of a solar cell is the ratio between maximum output power P_{max} to the incident power P_i :

$$\eta \equiv \frac{P_{max}}{P_i} = \frac{I_{sc} * V_{oc}}{P_i} * FF \tag{9.2}$$

Because of the wavelength and intensity dependence of P_{max}, the power conversion efficiency η should be measured under standard test conditions. For OSCs based on polymer: fullerene BHJ, the magnitude of Jsc, Voc and FF depends on light intensity [77], temperature [78][79], composition of components [80], thickness of active layer [81], choice of electrodes [81][82], as well as solid state morphology of thin film [84].

The basic measurement setup is shown in figure 9.1. A Keithley 2400 Source-Meter, controlled by LabVIEW program, is used for generating the voltage sweep and

measuring the resulting current through OSC. The OSC is connected in a four wire configuration to avoid parasitic serial resistance of the cables and interconnects on the substrate.

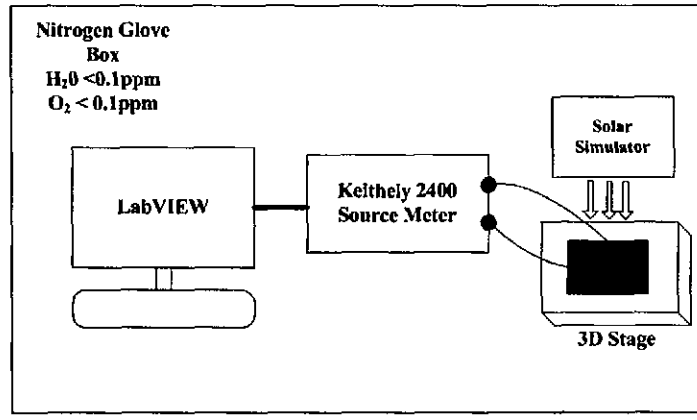

Figure 9.1. Basic IV measurement equipment block diagram. A LabVIEW controlled Keithley source meter used to record I-V curves of the OSC in a four wire configuration. Solar simulator equipped with xenon lamp, and 3D stage controller.

The solar simulator generates a spectrum close to 1sun condition. Before recording the IV-curve on the sun simulator, the illumination intensity is measured with reference to the solar cell and maintained at 1000 W/m^2. The temperatures for OSC measurements are maintained below 35^0C. The solar simulator system should be always concerned about two problems

1. Spectral mismatch with actual solar spectrum
2. Non uniform light intensity

First, the solar simulator gives out more light in the visible region where the polymer absorption spectrum peaks out. This will lead to mismatch with actual performance even if we set total irradiance of the simulator to the AM 1.5 solar irradiant ($100mW/cm^2$). The second is when non uniformity in light intensity of solar simulator. The intensity of lamp varies with time and distance even if source is held constant. Therefore, 3D positioning system is introduced to place a device to obtain consistent results every time.

Figure 9.2 shows J-V characteristics under AM 1.5 illumination for a calibrated solar simulator with an intensity of 100mW/cm^2 for P3HT:PCBM-C_{60}. Post production annealing is necessary to show photovoltaic effect in fabricated photovoltaic cells. Surprisingly, P3HT:PCBM-C_{70} shows more current density when compared to its analogous P3HT:PCBM-C_{60}. After annealing at 150^{0}C for 10minutes inside the nitrogen glove box J_{sc} and FF are improved significantly which leads to improved efficiency. Open circuit voltages Voc for the P3HT:PCBM-C_{70} cell were comparable to those of the P3HT:PCBM-C_{60}. After annealing improvement in the charge carrier transport network occurred in P3HT:PCBM-C_{70} as well as P3HT:PCBM-C_{60}. Jsc for P3HT:PCBM-C_{70} is more compared to P3HT:PCBM-C_{60}. One of the strategies for improvement of PV cell performance is the enhancement of the spectral coverage for sunlight. PCBM-C_{60} is not suitable as electron acceptor because of its very weak absorption peaks in the visible region. The analogous PCBM-C_{70} has wider range and strong absorption spectrum in the visible region which enhances PV performance. For PCBM-C_{60} is highly symmetric which decreases energy transitions. PCBM-C_{70} due to its asymmetry more transitions will take place inside active blend which dramatically improves light absorption [85]. This leads to improved charge separation and charge carrier density.

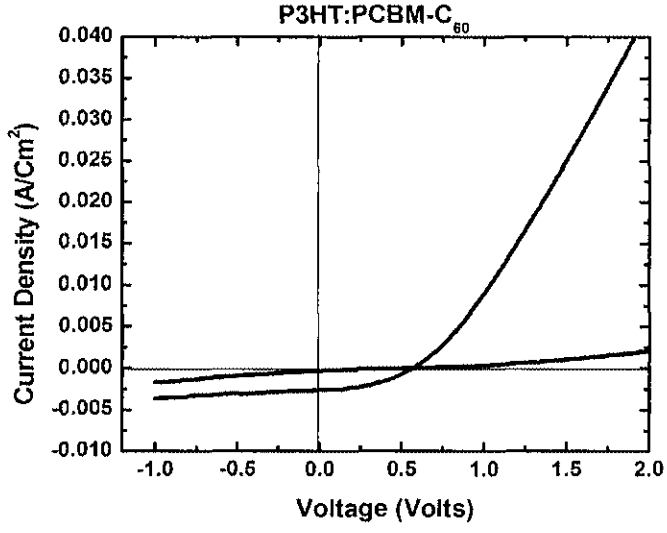

Figure 9.2. J-V characteristics (AM 1.5. 1000W/m^2) of unannealed and annealed P3HT: PCBM-C_{60} devices under illumination.

Typical J-V characteristics for P3HT: PCBM-C_{70} and P3HT: PCBM-C_{60} are shown in figure 9.3. The short-circuit current density (Jsc) and open-circuit voltage (Voc) are shown. The maximum output power (Pmax) is the area under the curve at its maximum voltage and current density.

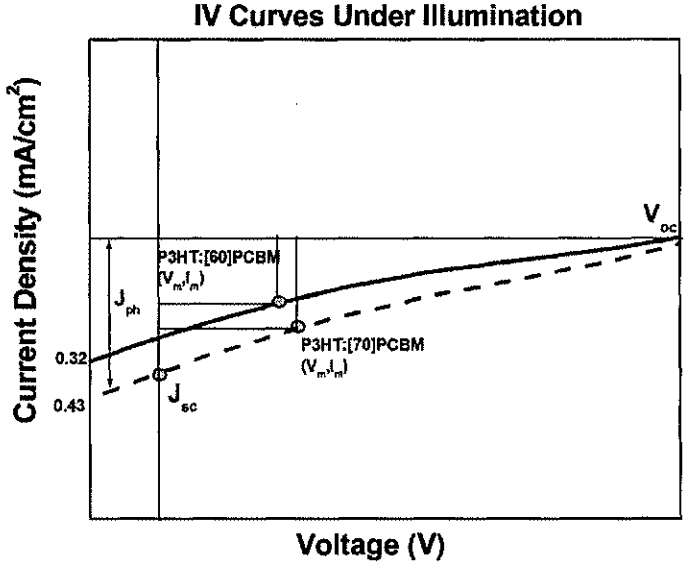

Figure 9.3. Typical J-V characteristics of P3HT: PCBM-C_{60} and P3HT: PCBM-C_{70} cells. The short-circuit current density (Jsc) and open-circuit voltage (Voc) are shown. The maximum output power (Pmax) is given by the rectangle Jm×Vm.

9.2 OPV Testing

The top electrode Al deposited using E-beam and immediately transferred to Nitrogen glove box with ppm levels less than 0.1ppm (H_20 and O_2) respectively without exposing its to the atmosphere. I-V measurements were taken by applying sweep voltage of -1V to 2V using a Keithley Source Meter. I-V curves are recorded using LabVIEW 8.2 from National Instruments.

An Oriel Newport light source with 300W range halogen lamp was used as a light source to measure IV characteristics. IR rays were filtered to avoid heating of photovoltaic device under testing and to get the exact solar spectrum.

The active area under consideration is different from the fabricated device. Figure 9.4 shows a cross sectional and top view schematic for the device under consideration to measure performance characteristics.

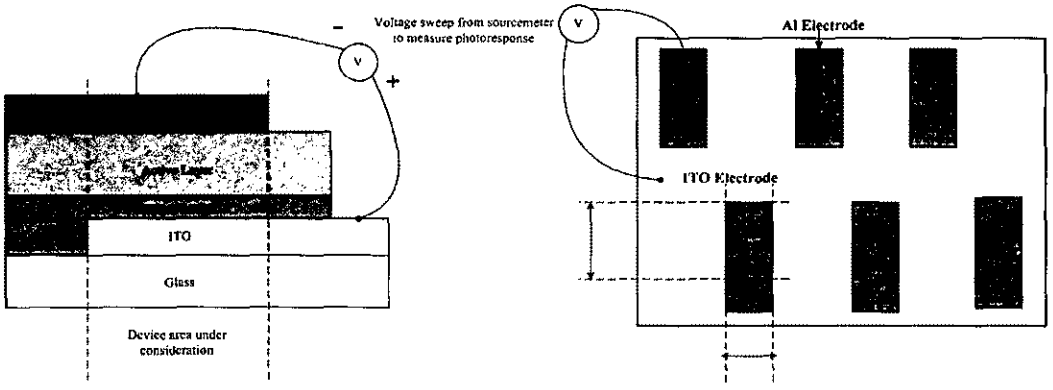

Figure 9.4. Cross sectional schematic and top view schematic of Organic Photo Voltaic (OPV). Region within dashed line indicates the actual region under consideration to measure performance characteristics of OPV. A sweep voltage is applied for OPV to determine IV characteristics. Aluminum overlapping region is only considered for forming a region where PV activity can be measured. ITO doesn't need to be patterned but Al electrode can be deposited using masking.

CHAPTER X

CONCLUSIONS & FUTURE WORK

10.1 CONCLUSIONS

In this work, correlation between structural and optical properties of polythiophene and polythiophene:fullerene films were studied using UV-Vis, Spectroscopy Ellipsometry and Atomic Force Microscope. Thin pristine polythiophene films were found to be partially crystalline. It was shown that annealing improves the overall crystallinity and anisotropy of the polythiophene films, because the fullerene molecules disturb the formation of the polythiophene crystallites. At elevated temperatures, the fullerene molecules become mobile and diffuse to the fullerene clusters. Due to the thermal diffusion of fullerene, regions with low fullerene concentration occur. In these fullerene-free regions, the polythiophene crystallizes upon annealing of the films. Due to the crystallization of polythiophene, the optical absorption and the hole mobility perpendicular to the film plane increases. The improved absorption of the annealed films together with improved transport properties result in increased polythiophene/fullerene solar cell efficiency. In this work we also report improved PV characteristics of Jsc by introducing PCBM-C_{70} as an acceptor. PCBM-C_{70} shows a stronger and wider absorption spectrum in the visible region than the analogus PCBM-C_{60}. Using PCBM-C_{70} we fabricated a highly efficient organic photovoltaic with higher power conversion efficiency. Therefore, we conclude that PCBM-C_{70} is a good and easy to replaceable alternative to PCBM-C_{60} with a better, wider absorption spectrum, and it will lead to higher performance PV cells.

10.2 FUTURE WORK

In future, photovoltaic cells efficient charge transfer can be done by nanopatterning active layer so that thickness of the layer can be decreased and dissociated charges are easily transferred to respective electrodes. P3HT is spin coated and free standing nanorods from the AAO template are used to make patterns, and PCBM fills in

those gaps. The top electrode Al is deposited, and post annealing treatment is done to show enhanced device performance.

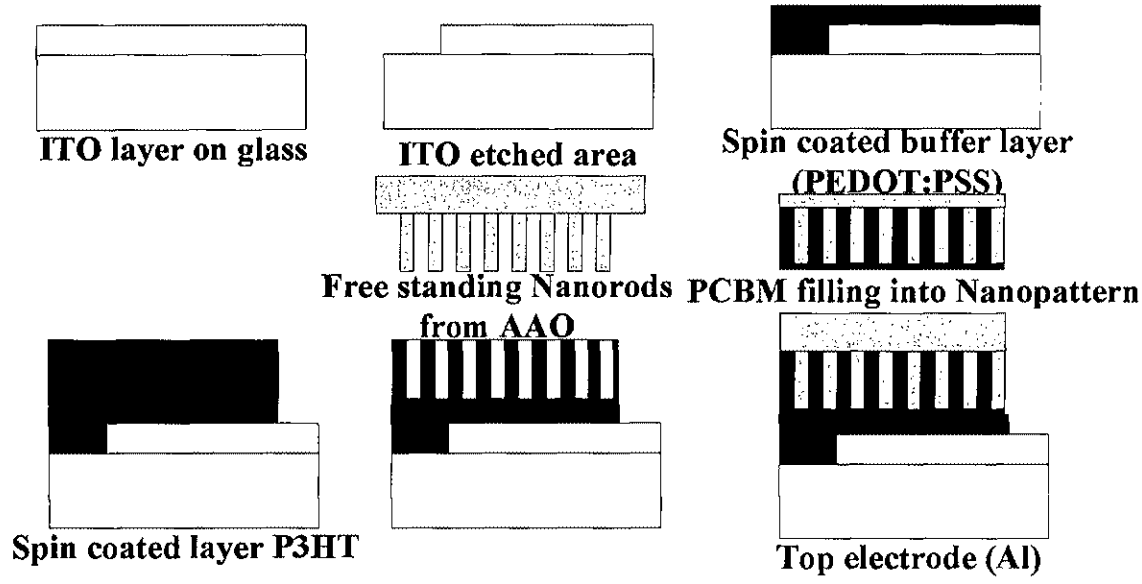

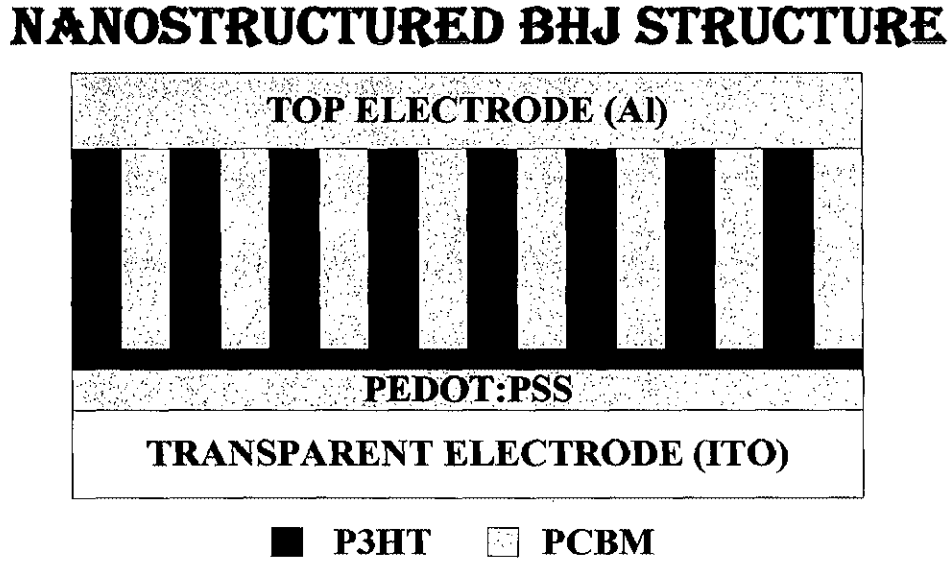

Figure 10.1. Step by step processing of nanostructured bulk heterojunction photovoltaic cell and its structure.

REFERENCES

[1] "Easing concerns about pollution from manufacture of solar cells", *Science Daily*, February 26, 2008.

[2] Dissertation by Moritz K. Riede, "Identification and Analysis of Key parameters in organic solar cells," Nov 2006.

[3] "Reported solar cell energy conversion efficiencies", National Renewable Energy Laboratory (USA).

[4] PHOTON International source, May 2006.

[5] Z. C. Liu, F. L. Xue, Y. Su, and K. Varahramyan, "Electrically bistable memory device based on spin-coated molecular complex thin film," *IEEE Electron Device Lett.*, Vol. 27, No. 3, pp. 151–153. 2006.

[6] G. Zerza, C. J. Brabec, G. Cerullo, S. De Silvestri, and N. S. Sariciftci, "Ultrafast charge transfer in conjugated polymer-fullerene composites," *Synthetic Metals*, Vol. 119, No. 1- 3, pp. 637-638, 2001.

[7] S-S.Sun, N.S.Sariciftci (eds.) Organic Photovoltaics, Taylor & Francis, London, 2005.

[8] Baigent, D.R., et al., "Conjugated Polymer Light Emitting Diodes on Silicon substrates," *Applied Phsyics Letters*, Vol. 65, No. 21, pp. 2636-2638, 1994.

[9] Sirringhaus, H., et al., "Mobility enhancement in conjugated polymer field effect transistors through chain alignment in a liquid-crystalline phase," *Applied Physics Letters*, Vol. 77, No. 3, pp. 406-408, 2000.

[10] Barton, M.I., et al., "Investigation of the TiO2/PPV nanocomposite for gas sensing applications," *Nanotechnology*, Vol. 9, No. 4, pp.356-359, 1998.

[11] Yu, G., K. Pakbaz, and A.J.Heeger, "Semiconducting Polymer Diodes – Large size Low Cost photodetectors with Excellent Visible Ultraviolet Sensitivity," *Applied Physics Letters*, Vol. 64, No. 25, pp.3422-3424, 1994.

[12] A. J. Heeger, "Semiconducting and metallic polymers: The fourth generation of polymeric materials," *Journal of Physical Chemistry B*, Vol. 105, No. 36, pp.8475-8491, 2001.

[13] G. Zerza, C. J. Brabec, G. Cerullo, S. De Silvestri, and N. S. Sariciftci, "Ultrafast charge transfer in conjugated polymer-fullerene composites," *Synthetic Metals*, Vol. 119, No. 1-3, pp.637-638, 2001.

[14] P. Peumans, A. Yakimov, and S. R. Forrest, "Small molecular weight organic thin-film photodetectors and solar cells," *Journal of Applied Physics* Vol. 93, No. 7, pp.3693–3723, 2003.

[15] Ray Swati, R. Banerjee, N. Basu, A. K. Batabyal, and A. K. Barua, "Properties of tin doped indium oxide thin films prepared by magnetron sputtering," *J. Appl. Phys.* Vol. 54, No. 6, pp.3497-3501, 1983.

[16] Gunes, S.; Neugebauer, H.; Sacriciftci, "Conjugated Polymer-Based Organic Solar Cells", *N. Chem. Rev.*, Vol. 107,No. 4, pp.1324-1338, 2007.

[17] L.Groenendaal, F.Jonas, D.Freitag, H.Pielartzik, and J.R.Reynolds, *Adv.Mater.* 12, 481 (2000).

[18] S.Ghosh, and O.Inganas, "Self-assembly of a conducting polymer nanostructure by physical crosslinking: applications to conducting blends and modified electrodes," *Synth.Met.*, Vol. 101, No. 1-3, pp.413-416, 1999.

[19] Commercial information from H.C.Starck can be found from www.hcstarck.com

[20] G.Greczynski, Th.Kulger, M.Keil, W.Osikowicz, M.Fahlman and W.R.Salaneck, "Photoelectron spectroscopy of thin films of PEDOT–PSS conjugated polymer blend: a mini-review and some new results," *J.Electron. Spectrosc. Relat. Phenom.*, Vol. 121, No. 1-3, pp.1-17, 2001.

[21] Wudl, *F.* "Fullerene Materials," *J. Mater. Chem.*, No.12, pp.1959-1963, 2002.

[22] Prato, M. "[60]Fullerene chemistry for materials science applications,"*J. Mater. Chem,* Vol. 7, pp. 1097, 1997.

[23] Y. Cao, G. Yu, C. Zhang, R. Menon, and A. J. Heeger, "Polymer lightemitting diodes with polyethylene dioxythiophene-polystyrene sulfonate as the transparent anode," *Synthetic Metals,* vol.87, pp.171-174, 1997.

[24] H. Hoppe, M. Niggemann, C. Winder, J. Kraut, R. Hiesgen, A. Hinsch, D. Meissner, and N. S. Sariciftci, "Nanoscale morphology of conjugated polymer/fullerene-based bulk-heterojunction solar cells," *Advanced Functional Materials*, Vol. 14, No. 10, pp.1005-1011, 2004.

[25] M. Al Ibrahim, O. Ambacher, S. Sensfuss, and G. Gobsch, "Effects of solvent and annealing on the improved performance of solar cells based on poly(3-hexylthiophene): Fullerene," *Applied Physics Letters*, Vol. 86, No. 20, pp.201120(1-3), 2005.

[26] D. Meyerhofer, "Characteristics of resist films produced by spinning," *Journal of Applied Physics*, Vol. 49, No. 7, pp.3993-3997, 1978.

[27] S. E. Shaheen, R. Radspinner, N. Peyghambarian, and G. E. Jabbour, "Fabrication of bulk heterojunction plastic solar cells by screen printing," *Applied Physics Letters*, Vol. 79, No. 18, 2001, pp. 2996-2998.

[28] T.Jeranko, H.Tributsch, N.S.Saricifti, J.C.Hummelen, "Patterns of efficiency and degradation of composite polymer cells," *Solar Energy Materials & Solar cells,* Vol. 83, No. 2-3 2004, pp. 247-262.

[29] D. Chirvase, J. Parisi, J. C. Hummelen, V. Dyakonov, "Influence of nanomorphology on the photovoltaic action of polymer-fullerene composites," *Nanotechnology*, Vol. 15, No. 9, 2004, pp. 1317-1323.

[30] N. Camaioni, G. Ridolfi, G. Casalbore-Miceli, G. Possamai, M. Maggini, "The effect of a mild thermal treatment on the performance of poly(3-allkylthiophene)/fullerene solar cells," *Advanced Materials*, Vol. 14, No. 23, 2002, pp. 1735-1738.

[31] X. Yang, J. Loos, S. C. Veenstra, W. J. H. Verhees, M. M. Wienk, J. M. Kroon, M. A. J. Michels, R. A. J. Janssen, "Nanoscale morphology of high-performance polymer solar cells," *Nano Letters,* Vol. 5, No. 4, 2005, pp. 579-583.

[32] K. J. Ihn, J. Moulton, P. Smith, "Whiskers of poly(3-alkylthiophene)s," *Journal of Polymer Science Part B-Polymer Physics,* Vol. 31, pp. 735-742, 1993.

[33] S.Malik, A. K.Nandi, "Crystallization mechanism of regioregular poly(3-alkyl thiophene)s," *Journal of Polymer Science Part B-Polymer Physics,* Vol. 40, No. 18, pp. 2073-85, 2002.

[34] E. Mena-Osteritz, A. Meyer, B. M. W. Langeveld-Voss, R. A. J. Janssen, E. W. Meijer, P. Bauerle, "Two-dimensional crystals of poly(3-alkylthiophene)s: Direct visualization of polymer folds in submolecular resolution," *Angew. Chem. International Edition,* Vol. 39, No. 15, pp. 2680-84, 2000.

[35] H. Sirringhaus, P. J. Brown, R. H. Friend, M. M. Nielsen, K. Bechgaard, B. M. W. Langeveld-Voss, A. J. H. Spiering, R. A. J. Janssen, E. W. Meijer, P. Herwig and D. M. de Leeuw, "Two-dimensional Charge transport in self-organized high-mobility conjugated polymers," *Nature* Vol. 401, pp. 685-688, 1999.

[36] G. Dicker et al., "Photoconductivity enhancement of P3HT by increasing inter and intra chain order", *Synthetic Metals*, Vol. 137, No. 1-3, pp. 863-864, 2003.

[37] X. Yang, J. Loos, S. C. Veenstra, W. J. H. Verhees, M. M. Wienk, J. M. Kroon, M. A. J. Michels and R. A. J. Janssen, "Nanoscale morphology of high-performance polymer solar cells, " *Nano Lett.* Vol. 5, No. 4, pp. 579-583, 2005.

[38] S. Marchaut and P. J. S. Foot, "Annealing behavior of conductive poly(3-hexylthiophene)," *Polymer,* Vol. 38, No. 7, pp.1749-51, 1997.

[39] Zhang Cai Rong etc.al, "DFT Study on Methanofullerene Derivative [6,6]-Phenyl-C_{61} Butyric Acid Methyl Ester," *Acta Phys. Chim. Sin.,* 24 (X), pp. 001-009, 2008.

[40] S. Hugger, R. Thomann, T. Heizel and T. Thurn-Albiecht, "Semicrystalline morpholoty in thin films of poly(3-hexylthiophene)," *Colloid Polym Sci.* Vol. 282, No. 4, pp.932-938, 2004.

[41] D. Meschede, Gerthsen Physik Springer, Berlin, 2002.

[42] H. Sirringhaus, R. J. Wilson, R. H. Friend, M. Inbasekaran, W. Wu, E. P. Woo, M. Grell, D. D. C. Bradley, "Mobility enhancement in conjugated polymer field-effect transistors through chain alignment in a liquid-crystalline phase," *Appl. Phys. Lett.* Vol. 77, No. 3, pp.406-408, 2000.

[43] P. Gattinger, H. Rengel, D. Neher, M. Gurka, M. Buck, A. M. van de Craats, J. M. Warman, "Mechanism of Charge Transport in Anisotropic Layers of a Phythalocyanine Polymer" *J. Phys. Chem. B,* Vol. 103, No. 16, pp.3179-86, 1999.

[44] E. Punkka, M. F. Rubner, "Formation of rectifying contacts to Langmuir-Blodgett films of poly(3-hexylthiophene)," *Synth. Met.*, Vol. 42, No. 1-2, pp.1509-1513, 1991.

[45] Guide to using WVASE32 (J. A. Woollam co., Inc., 1995).

[46] D. McBranch, I. H. Campbell, D. L. Smith, J. P. Ferraris, "Optical determination of chain orientation in electroluminescent polymer films," *Appl. Phys. Lett.*, Vol. 66, pp.1175, 1995.

[47] L. A. A. Pettersson, F. Carlsson, O. Inganas, H. Arwin, "Spectroscopic Ellipsometry Studies of Optical Properties of Doped Poly(3,4-ethylenedioxythiophene): An Anisotropic Metal," *Thin Solid Films,* Vol. 313- 314, No. 1-2, pp.356-61, 1998.

[48] R. W. Gymer, R. H. Friend, H. Ahmed, P. L. Burn, A. M. Kraft, A. B. Holmes, "The Fabrication and Assessment of Optical Waveguides in Poly (p-phenylenevinylene)/ Poly(2,5-dimethoxy –P-phenylenevinylene) Copolymer," *Synth. Met.*, Vol. 55-57, pp.3683-88, 1993.

[49] J. Sturm, S. Tasch, A. Niko, G. Leising, E. Toussaere, J. Zyss, T. C. Kowalczyk, K. D. Singer, U. Scherf, J. Huber, "Optical anisotropy in thin films of a blue electroluminescent conjugated polymer," *Thin Solid Films,* Vol. 298, pp.138-142, 1997.

[50] M. Tammer, P. Monkman, "Measurement of the Anisotropic Refractive Indices of Spin Cast Thin Poly(2-methoxy-5-(2-ethyl-hexyloxy)-*p*-phenylenevinylene) (MEH-PPV) Films," *Adv. Mat.*, Vol. 14, No. 3, pp.210-12, 2002.

[51] C. M. Ramsdale, N. C. Greenham, "Ellipsometric Determination of Anisotropic Optical Constants in Electroluminescent Conjugated Polymers,"*Adv. Mat.* Vol. 14, No. 3, pp.212-15, 2002.

[52] W. A. Mcgahan, B. R. Spady, J. A. Iacoponi and J. D. Williams, "Combined spectroscopic ellipsometry and reflectometry for advanced semiconductor fabrication metrology," *Proc. SPIE,* Vol. 2877, pp.132-41, 1996.

[53] G.E.Jellison, "Spectroscopic ellipsometry data analysis: measured versus calculated quantites," *Thin Solid Films*, Vol. 313-314, No. 1-2, pp.33-39, 1998.

[54] (www.nanoscience.com/education/AFM.html)

[55] PhD Dissertation by Harald Hoppe, "Nanomorphology – Efficiency Relationship in Organic Bulk Heterojunction Plastic Solar cells," Johannes Kepler University, October 2004.

[56] G. Binning, C. F. Quate, "Atomic Force Microscope," *Phys. Rev. Lett.*, Vol. 56, No. 9, pp.930-933, 1986.

[57] M. Berggren, G. Gustafsson, O. Inganas, M. R. Andersson, O. Wennerstrom and T. Hjerberg, "Thermal control of near-infrared and visible electroluminescence in alkyl-phenyl substituted polythiophenes," *Appl. Phys. Lett.*, Vol. 65, No. 12, pp.1489, 1994.

[58] N. Camaioni, G. Ridolfi, G. Casalbore-Miceli, G. Possamai and M. Maggini, "The Effect of a Mild Thermal Treatment on the Performance of Poly(3-alkylthiophene)/Fullerene Solar Cells ," *Adv. Mater.*, Vol. 14, No. 23, pp.1735-38, 2002.

[59] G. Li, V. Shrotriya, J. Huang, Y. Yao, T. Moriarty, K. Emery and Y. Yang, "High-efficiency solution processable polymer photovoltaic cells by self-organization of polymer blends," *Nat. Mater.*, Vol. 4, pp.864-868, 2005.

[60] W. Ma, C. Yang, X. Gong, K. Lee and A. J. Heeger, "Thermally Stable, Efficient Polymer Solar Cells with Nanoscale Control of the Interpenetrating Network Morphology," *Adv. Funct. Mater.*, Vol. 15, No. 10, pp.1617-22, 2005.

[61] M. Reyes-Reyes, K. Kim and D. L. Carroll, "High-efficiency photovoltaic devices based on annealed poly(3-hexylthiophene) and 1-(3-methoxycarbonyl)-propyl-1- phenyl-(6,6)C_{61} blends" *Appl. Phys. Lett.*, Vol. 87, No. 8, 083506(1-3), 2005.

[62] Y. Kim, S. Cook, S. M. Tuladhar, S. A. Choulis, J. Nelson, J. R. Durrant, D. D. C. Bradley, M. Giles, I. McCulloch, C.-S. Ha and M. Ree, "A strong regioregularity effect in self-organizing conjugated polymer films and high-efficiency polythiophene:fullerene solar cells" *Nat. Mater.*, Vol. 5, pp.197-203, 2006.

[63] L. S. Roman, M. R. Andersson, T. Yohannes, and O. Ingana¨s, "Photodiodes performance and nanostructure of polythiophene/C60 blends," *Advanced Materials*, Vol. 9, No. 15, pp. 1164-1168, 1997.

[64] S. E. Shaheen, C. J. Brabec, N. S. Sariciftci, F. Padinger, T. Fromherz, and J. C. Hummelen, "2.5% Efficient organic plastic solar cells," *Applied Physics Letters*, Vol. 78, No. 6, pp.841-843, 2001.

[65] J. J. Halls, C. A. Walsh, N. C. Greenham, E. A. Marseglia, R. H. Friend, S. C. Moratti, and A. B. Holmes, "Efficient photodiodes from interpenetrating polymer networks," *Nature*, Vol. 376, No. 6540, pp.498-500, 1995.

[66] C. Y. Yang and A. J. Heeger, "Morphology of composites of semiconducting polymers mixed with C_{60}," *Synthetic Metals*, Vol. 83, No. 2, pp.85-88, 1996.

[67] M. T. Rispens, A. Meetsma, R. Rittberger, C. J. Brabec, N. S. Sariciftci, and J.C.Hummelen, "Influence of the solvent on the crystal structure of PCBM and the efficiency of MDMO-PPV: PCBM 'plastic' solar cells," *Chemical Communications*, Vol. 17, pp.2116-2118, 2003.

[68] E. A. Katz, D. Faiman, S. M. Tuladhar, J. M. Kroon, M. M Wienk, T. Fromherz, F. Padinger, C.J. Brabec, and N.S. Sariciftci, "Temperature dependence for the photovoltaic device parameters of polymer-fullerene solar cells under operating conditions," *J. Appl. Phys.*, 90, pp.5343-5350, 2001.

[69] I. Riedel, J. Parisi, V. Dyakonov, L. Lutsen, D. Vanderzande, and J. C. Hummelen, "Effect of Temperature and Illumination on the Electrical Characteristics of Polymer-Fullerene Bulk-Heterojunction Solar Cells ,"*Adv. Func. Mater,* Vol. 14, No. 1, pp.38-44, 2004.

[70] X. Yang, J. Loos, S. C. Veenstra, W. J. H. Verhees, M. M. Wienk, J. M. Kroon, M. A. J. Michels, R. A. J. Janssen, "Nanoscale morphology of high-performance polymer solar cells," *Nano Letters,* Vol. 5, No. 4, pp.579-583, 2005.

[71] K. J. Ihn, J. Moulton, P. Smith, "Whiskers of poly(3-alkylthiophene)s," *Journal of Polymer Science Part B-Polymer Physics,* Vol. 31, pp.735-742, 1993.

[72] S.Malik, A. K.Nandi, "Crystallization mechanism of regioregular poly(3-alkyl thiophene)s," *Journal of Polymer Science Part B-Polymer Physics,* Vol. 40, No. 18, pp.2073-85, 2002.

[73] Y. Kanemitsu, K. Suzuki, Y. Masumoto, Y. Tomiuchi, Y. Shiraishi, M. Kuroda, "Optical properties of quasi-one-dimensional thiophene-based oligomers," *Phys. Rev. B*, Vol. 50, No. 4, pp.2301-2305, 1994.

[74] G. Padmanaban, S. Ramakrishan, "Conjugation Length Control in Soluble Poly[2-methoxy-5-((2'-ethylhexyl)oxy)-1,4-phenylenevinylene] (MEHPPV): Synthesis, Optical Properties, and Energy Transfer," *J. Am. Chem. Soc.,* Vol. 122, pp.2244-2251, 2000.

[75] E. Mena-Osteritz, A. Meyer, B. M. W. Langeveld-Voss, R. A. J. Janssen, E. W. Meijer, P. Bauerle, "Two-dimensional crystals of poly(3-alkylthiophene)s: Direct visualization of polymer folds in submolecular resolution," *Angewandte Chemie-International Edition*, Vol. 39, No. 15, pp.2680-2684, 2000.

[76] Youngkyoo kim, Jenny Nelson, James R.Durrant "Polymer chain/nanocrystal ordering in thin films of P3HT and blends with a soluble fullerene," *Soft Matter*, Vol. 3, pp.117-121, 2007.

[77] P. Schilinsky, C.Waldauf, C. J. Brabec, "Recombination and loss analysis in polythiophene based bulk heterojunction photodetectors," *Applied Physics Letters*, Vol. 81, No. 20, pp.3885-87, 2002.

[78] V. Dyakonov, "Electrical aspects of operation of polymer-fullerene solar cells," *Thin Solid Films*, Vol. 451-452, pp.451-52, 2004.

[79] I. Riedel, J. Parisi, V. Dyakonov, L. Lutsen, D. Vanderzande, J. C. Hummelen, "Effect of temperature and illumination on the electrical characteristics of polymer-fullerene bulk- heterojunction solar cells," *Advanced Functional Materials*, Vol. 14, No. 1, pp.38-44, 2004.

[80] J. K. J. van Duren, X. N. Yang, J. Loos, C. W. T. Bulle-Lieuwma, A. B. Sieval, J. C. Hummelen, R. A. J. Janssen, "," *Advanced Functional Materials,* Vol. 14, No. 5, pp.425-34, 2004.

[81] H. Hoppe, N. Arnold, N. S. Sariciftci, D. Meissner, "Modeling the optical absorption within conjugated polymer/fullerene-based bulk-heterojunction organic solar cells," *Solar Energy Materials and Solar Cells*, Vol. 80, No. 1, pp.105-113, 2003.

[82] C. J. Brabec, A. Cravino, D. Meissner, N. S. Sariciftci, M. T. Rispens, L. Sanchez, J. C. Hummelen, T. Fromherz, "The influence of materials work function on the open circuit voltage of plastic solar cells," *Thin Solid Films*, Vol. 403-404, pp.368-372, 2002.

[83] C. J. Brabec, S. E. Shaheen, C. Winder, N. S. Sariciftci, P. Denk, "Effect of LiF/metal electrodes on the performance of plastic solar cells," *Applied Physics Letters,* Vol. 80, No. 7, pp. 1288-90, 2002.

[84] S. E. Shaheen, C. J. Brabec, N. S. Sariciftci, F. Padinger, T. Fromherz, and J. C. Hummelen, "2.5% Efficient organic plastic solar cells," *Applied Physics Letters*, Vol. 78, No. 6, pp.841-843, 2001.

[85] M.M.Wienk, J.M.Kroon, W.J.H.Verhees, J.Knol, J.C.Hummelen, P.A.Van Hal and R.A.J.Janssen, "Efficient Methano[70]fullerene/MDMO-PPV Bulk Heterojunction Photovoltaic Cells," *Angew. Chem.*, Int.Ed. Vol. 42, pp.3371-3375, 2003.

VITA

SRI SABARINADH SUNKAVALLI

EDUCATION

Master of Science Electrical and Computer Engineering, Old Dominion University

Bachelor of Science Electrical & Electronics Engineering, Andhra University

SKILLS SUMMARY

Semiconductor devices fabrication techniques - DC & RF Sputtering, Photolithography, E-beam Evaporation, Thermal Evaporation, Rapid thermal annealer (RTA), Electron beam lithography

High vacuum deposition techniques - Molecular Beam Epitaxy (MBE) for the growth of organic and inorganic materials.

Semiconductor characterization techniques - Atomic Force Microscopy (AFM), X-ray diffraction (XRD) measurement, Scanning Electron Microscope (SEM), Transmission Electron Microscope (TEM), Dektak surface profiler

Optical and electrical characterization - UV-Vis-IR Spectrophotometer, VASE Spectroscopic Ellipsometry.

Analysis & Simulation of real time problems using MATLAB, Instrument control and Data acquisition using LabVIEW, Custom integrated circuit design using CADENCE.

AWARDS & ACTIVITIES

- ✓ Secured **first prize** in poster competition at Jefferson Lab, Newport News.
- ✓ Awarded with "***Honorable Mention***" in Research Expo conducted at Old Dominion University where 8 schools participated.
- ✓ **IEEE** student chapter Leader 2003.
- ✓ Organized & participated in **TECHFEST-2005, 2006** a National level Technical paper presentation contest conducted at our college.
- ✓ Active member of **IETE** (The *Institute of Electronics and Telecommunication Engineers*).
- ✓ Active member of **CRRAZE** (*C R Reddy Association for Zooming Electrical*), an organization of likeminded Electrical Engineers in our college.